

UNDERSTANDING MATRIX FUNCTION NORMALIZATIONS IN COVARIANCE POOLING THROUGH THE LENS OF RIEMANNIAN GEOMETRY

Anonymous authors

Paper under double-blind review

ABSTRACT

Global Covariance Pooling (GCP) has been demonstrated to improve the performance of Deep Neural Networks (DNNs) by exploiting second-order statistics of high-level representations. GCP typically performs classification of the covariance matrices by applying matrix function normalization, such as matrix logarithm or power, followed by a Euclidean classifier. However, covariance matrices inherently lie in a Riemannian manifold, known as the Symmetric Positive Definite (SPD) manifold. The current literature does not provide a satisfactory explanation of why Euclidean classifiers can be applied directly to Riemannian features after the normalization of the matrix power. To mitigate this gap, this paper provides a comprehensive and unified understanding of the matrix logarithm and power from a Riemannian geometry perspective. The underlying mechanism of matrix functions in GCP is interpreted from two perspectives: one based on tangent classifiers (Euclidean classifiers on the tangent space) and the other based on Riemannian classifiers. Via theoretical analysis and empirical validation through extensive experiments on fine-grained and large-scale visual classification datasets, we conclude that the working mechanism of the matrix functions should be attributed to the Riemannian classifiers they implicitly respect.

1 INTRODUCTION

Global Covariance Pooling (GCP), a method used as a replacement for Global Average Pooling (GAP) in aggregating the final activations of Deep Neural Networks (DNNs), has demonstrated exceptional performance improvements across a variety of applications (Lin et al., 2015; Ionescu et al., 2015; Li et al., 2017; Wang et al., 2017; Koniusz et al., 2017; Li et al., 2018; Wang et al., 2020a; Rahman et al., 2020; Zhu et al., 2024). The research line of existing GCP methods mainly focuses on improving performance by adopting different normalization methods (Ionescu et al., 2015; Li et al., 2017; Wang et al., 2020a), exploiting richer statistics (Cui et al., 2017; Wang et al., 2017; Koniusz et al., 2021; Rahman et al., 2023), improving covariance conditioning (Song et al., 2022d;a), and obtaining compact representations (Gao et al., 2016; Yu & Salzmann, 2018; Lin et al., 2018; Wang et al., 2022a). Generally speaking, a GCP meta-layer computes the covariance matrix of the activations as the global representation, and then performs normalization either by *matrix logarithm* (Ionescu et al., 2015) or *matrix power* (Li et al., 2017; 2018; Wang et al., 2020a). Finally, the normalized matrices are fed into a Euclidean classifier. The square root has emerged as the most effective normalization scheme, outperforming the logarithm counterpart by a large margin (Li et al., 2017; Wang et al., 2020a; Song et al., 2021). The research community has provided some theoretical support for the matrix logarithm. However, there are no intrinsic explanations for the matrix power.

The covariance matrices naturally lie in a Riemannian manifold, known as Symmetric Positive Definite (SPD) manifolds (Pennec et al., 2006). For matrix logarithm, it maps SPD matrices into the Euclidean space of the tangent space at the identity matrix. Euclidean classifiers can, therefore, be applied after the matrix logarithm. However, the co-domain of the matrix power is still the SPD manifold, rendering the application of Euclidean classifiers following matrix power less mathematically supported. Several works have attempted to explain the matrix power. The initial motivation of matrix power in GCP (Li et al., 2017) is that the distance induced by the matrix square root approximates the geodesic distance under Log-Euclidean Metric (LEM) (Dryden et al., 2010). Never-

theless, Fig. 1 shows that the gap between these two distances is still noticeable. Furthermore, Song et al. (2021) empirically explored the benefits of approximate matrix square root over its accurate counterpart, while Wang et al. (2020b) studied the merits of GCP from an optimization perspective. *However, none of them touch upon the fundamental reason why Euclidean classifiers can be directly employed in the non-Euclidean co-domain of the matrix power.* There appears to be a discrepancy between theoretical principles and practical applications of matrix power and logarithm.

This study aims to offer a comprehensive theoretical understanding of the matrix logarithm/power in GCP and reconcile the discrepancy between theory and practice. Without loss of generality, we refer to matrix logarithm and power collectively as matrix functions. Given that the matrix logarithm is a Riemannian logarithmic map, mapping SPD data into the tangent space, we first systematically study Riemannian logarithmic maps on SPD manifolds under seven families of metrics, resulting in three types of Riemannian logarithmic maps, the ones based on the matrix logarithm, matrix power, and Log-Cholesky Metric (LCM), respectively. Consequently, the matrix logarithm in GCP establishes a tangent classifier (Euclidean classifiers on the tangent space) for covariance classification. Also, by applying a simple affine transformation, the matrix power in GCP constructs a tangent classifier. This indicates that we might unify both matrix logarithm and power as tangent classifiers. However, our experiments suggest that this tangent classifier explanation fails to account for the efficacy of matrix power. As the tangent space distorts the intrinsic geometry of manifolds, we conjecture that tangent classifiers might not be the underlying mechanisms.

To delve further, we move on to a more intrinsic explanation based on the recently developed SPD Multinomial Logistics Regression (MLR) (Nguyen & Yang, 2023; Chen et al., 2024a;c), which extends the Euclidean MLR (FC + softmax) into manifolds. Based on previous work (Chen et al., 2024a), we find that matrix logarithm in GCP implicitly constructs the SPD MLR under LEM. Furthermore, we theoretically demonstrate that the matrix power in GCP implicitly respects the SPD MLR under PEM. These findings suggest that matrix functions in GCP can be uniformly interpreted as Riemann classifiers. Therefore, the observed performance gap between the matrix power and logarithm can be attributed to the characteristics of the underlying Riemannian metrics. To validate this postulation, we conduct experiments on the ImageNet-1k (Deng et al., 2009) and three Fine-Grained Visual Categorization (FGVC) datasets, namely Caltech University Birds (Birds) (Welinder et al., 2010), Stanford Cars (Cars) (Krause et al., 2013), and FGVC Aircrafts (Aircrafts) (Maji et al., 2013). *The results confirm that the Riemannian classifier rather than the tangent classifier contributes to the efficacy of matrix functions in GCP. We expect our work to pave the way for a deeper theoretical understanding of GCP from a Riemannian perspective and inspire more research to explore the rich SPD geometries for more effective GCP applications.* We present a teaser table in Tab. 1. Due to page limits, we put the related work in App. B and all the proofs in the appendix. Besides, tables of notations and abbreviations are presented in App. C for better readability.

In summary, our main **contributions** are two-fold. **(a). First intrinsic explanation for matrix normalization.** We explain the working mechanism of matrix functions in GCP from the perspectives of tangent and Riemannian classifiers, and finally claim that the rationality of matrix functions should be attributed to the Riemannian classifiers they implicitly respect. To the best of our knowledge, this is the first Riemannian interpretation of the matrix functions in GCP. **(b). Empirical validation by extensive experiments.** We validate our theoretical argument on large-scale and FGVC datasets.

Main theoretical results: Tab. 2 presents a complete list of Riemannian logarithmic maps on SPD manifolds under different metrics. It indicates that the matrix power, with a simple affine transformation, can serve as a Riemannian logarithmic map. Since the matrix logarithm has been widely recognized as a building component of tangent classifiers, we also expect that the matrix power function can be explained by tangent classifiers. However, the preliminary experiments presented in

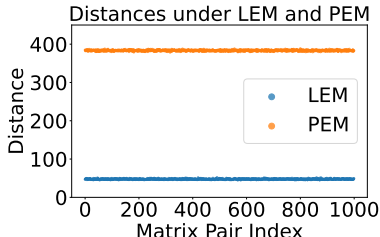


Figure 1: The metric induced by the matrix power is the Power Euclidean Metric (PEM). Although PEM approaches LEM as the power approaches 0, the distances under PEM ($\theta = 0.5$) and LEM still differ largely. We visualize these two distances for 1000 random pairs of 256×256 SPD matrices. The average difference is 335.84 ± 1.61 . *This indicates that matrix power is not proximate to LEM for classification under the widely used $\theta = 0.5$.*

Table 1: **Main results:** The working mechanisms of matrix functions in GCP are attributed to Riemannian classifiers they implicitly respect.

Matrix function	Intrinsic explanation	Used in GCP	Reference
Logarithm	LEM-induced Riemannian Classifier	Log-EMLR (Eq. (4))	(Chen et al., 2024a, Prop. 5.1)
Power	PEM-induced Riemannian Classifier	Pow-EMLR (Eq. (5))	Thm. 2

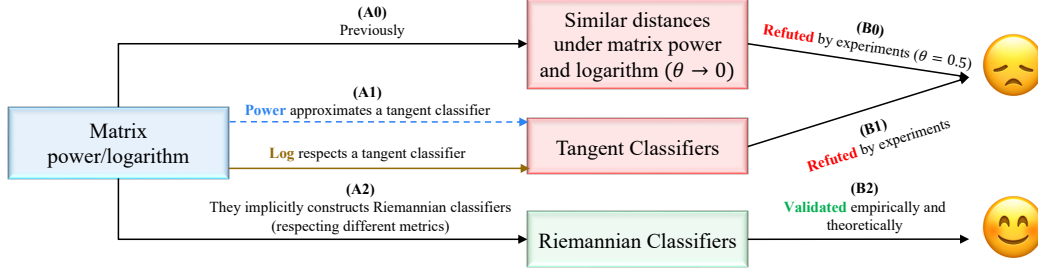


Figure 2: Illustration on the main postulations (A0 to A2) and empirical validations (B0 to B2) of our investigation, where θ is the power in the matrix power. Postulation **A0** is adopted by (Li et al., 2017) and is refuted by our experiments in Fig. 1 for the specific $\theta = 0.5$. Postulation **A1** is indicated by Tab. 2 and is refuted by our experiments in Sec. 6. Postulation **A2** is supported by Thm. 2 and is validated by our experiments in Sec. 6.

Tab. 3 refute this conjecture, suggesting the existence of more fundamental mechanisms. Therefore, we delve into this mystery in Sec. 5 by leveraging the recently developed Riemannian classifiers. *Thm. 2 indicates that matrix power in GCP implicitly establishes a Riemannian classifier for covariance matrix classification.* Similar results also hold for the matrix logarithm (Chen et al., 2024a). This implies that the matrix logarithm and power can be unifiedly interpreted as essential components of Riemannian classifiers. Tab. 4 summarizes all our theoretical findings. Sec. 6 further validate our theoretical explanations by extensive experiments. The reasoning behind our analysis is illustrated in Fig. 2.

2 THE GEOMETRY OF SPD MANIFOLDS

Let \mathcal{S}_{++}^n be the set of $n \times n$ SPD matrices. As shown by Arsigny et al. (2005), \mathcal{S}_{++}^n is an open submanifold of the Euclidean space \mathcal{S}^n of symmetric matrices. There are five popular Riemannian metrics on SPD manifolds: Affine-Invariant Metric (AIM) (Pennec et al., 2006), Log-Euclidean Metric (LEM) (Arsigny et al., 2005), Power-Euclidean Metric (PEM) (Dryden et al., 2010), Log-Cholesky Metric (LCM) (Lin, 2019), and Bures-Wasserstein Metric (BWM) (Bhatia et al., 2019). Note that when power equals 1, PEM reduces to the Euclidean Metric (EM). All of the above five standard metrics have been generalized into parameterized families of metrics.

Thanwerdas & Pennec (2023) generalized AIM, LEM, and EM into two-parameter metrics by the $O(n)$ -invariant Euclidean inner product on \mathcal{S}^n :

$$\langle V, W \rangle^{(\alpha, \beta)} = \alpha \langle V, W \rangle + \beta \text{tr}(V) \text{tr}(W), \quad (1)$$

where $\alpha > 0$ and $\beta > -\alpha/n$, $V, W \in \mathcal{S}^n$, and $\langle \cdot, \cdot \rangle$ is the standard matrix inner product. These generalized metrics are denoted as (α, β) -AIM, (α, β) -LEM, and (α, β) -EM, respectively. Besides, Thanwerdas & Pennec (2022) defined the power-deformed metric \tilde{g} of a metric g on \mathcal{S}_{++}^n as

$$\tilde{g}_P(V, W) = \frac{1}{\theta^2} g_{P^\theta}((\text{Pow}_\theta)_{*,P}(V), (\text{Pow}_\theta)_{*,P}(W)), \forall P \in \mathcal{S}_{++}^n, V, W \in T_P \mathcal{S}_{++}^n, \quad (2)$$

where $\text{Pow}_\theta(P) = P^\theta$ denotes matrix power, $(\text{Pow}_\theta)_{*,P}$ is the differential map of Pow_θ at P , and $T_P \mathcal{S}_{++}^n$ is the tangent space at P . Following Eq. (2), (α, β) -AIM, (α, β) -LEM, (α, β) -EM, LCM, and BWM are generalized into power-deformed families of metrics, denoted as (θ, α, β) -AIM, (θ, α, β) -LEM, (θ, α, β) -EM, θ -LCM, and 2θ -BWM, respectively (Thanwerdas & Pennec, 2022; Chen et al., 2024c). Chen et al. (2024c) further shows that (θ, α, β) -LEM equals (α, β) -LEM. Besides, as shown by Thanwerdas & Pennec (2022); Chen et al. (2024c), θ serves as a deformation from

a LEM-like metric. For instance, (θ, α, β) -AIM becomes (α, β) -AIM when $\theta = 1$ and approaching (α, β) -LEM with $\theta \rightarrow 0$.

On the other hand, PEM was generalized into Mixed Power Euclidean Metric (MPEM) (Thanwerdas & Pennec, 2019) by two power factors θ_1 and θ_2 , denoted as (θ_1, θ_2) -EM. When $\theta_1 = \theta_2$, MPEM is reduced to PEM. Han et al. (2023) extended BWM into Generalized Bures-Wasserstein Metric (GBWM) by an SPD parameter M , denoted as M -BWM. When $M = I$, GBWM is reduced to BWM. We further generalize GBWM into $(2\theta, M)$ -BWM by power deformation Eq. (2).

In total, three parameters (θ, α, β) are involved in the metrics on the SPD manifold. The power deformation θ characterizes deformation (Chen et al., 2024c; Thanwerdas & Pennec, 2022), while (α, β) characterizes the $O(n)$ -invariance, a powerful property in modeling covariance (Thanwerdas & Pennec, 2023). The above metrics have shown success in various applications, due to their closed-form expressions for Riemannian operators, such as the Riemannian logarithmic and exponential maps. We summarize the involved Riemannian operators in App. D.2.

3 GLOBAL COVARIANCE POOLING REVISITED

GCP captures the second-order statistics of the features in the last layer of the deep network. The standard GCP procedure comprises calculating the covariance matrix, normalization with a matrix function, vectorization, dimensionality reduction by an FC layer, and ultimately applying a Euclidean classifier. The sequence of these operations can be represented as follows:

$$X \xrightarrow{\text{Cov}} \Sigma \xrightarrow{f_M} \tilde{\Sigma} \xrightarrow{f_{\text{vec}}} x \xrightarrow{f_{\text{FC}}} \tilde{x} \xrightarrow{f_{\text{EC}}} \hat{y}, \quad (3)$$

where f_M , f_{vec} , f_{FC} and f_{EC} denote the matrix function, vectorization, FC layer, and Euclidean classifier, respectively. Typical candidates of matrix functions are matrix power and logarithm. As softmax is the most widely used classifier, f_{EC} always denotes the softmax in this paper. However, our discussions can also apply to other classifiers used in GCP, such as SVM (Li et al., 2017; Wang et al., 2020a), as other classifiers receive the FC features as their inputs.

FC + softmax is known as Euclidean Multinomial Logistics Regression (EMLR). When the matrix function is the matrix power, we call the process $f_{\text{EC}} \circ f_{\text{FC}} \circ f_{\text{vec}} \circ f_M$ as the Pow-EMLR, while the counterpart of matrix logarithm is referred to as Log-EMLR. Especially, setting power as $1/2$ in GCP normally reaches the optimal performance (Li et al., 2017, Fig. 3). The Pow-EMLR and Log-EMLR can be formally expressed as

$$\text{Log-EMLR: } \text{softmax}(\mathcal{F}(f_{\text{vec}}(\text{mlog}(S)); A, b)), \quad (4)$$

$$\text{Pow-EMLR: } \text{softmax}(\mathcal{F}(f_{\text{vec}}(S^\theta); A, b)), \quad (5)$$

where $\mathcal{F}(\cdot; A, b)$ denotes the FC layer with the transformation matrix A and biasing vector b .

4 MATRIX FUNCTIONS AND TANGENT CLASSIFIERS

The matrix logarithm is the Riemannian logarithmic map at the identity matrix I , mapping SPD matrices into the tangent space $T_I \mathcal{S}_{++}^n \cong \mathcal{S}^n$. As tangent spaces are Euclidean spaces, it is natural to exploit FC and Euclidean classifiers on $T_I \mathcal{S}_{++}^n$ directly. We refer to the Euclidean classifiers over the tangent space at the identity matrix, $T_I \mathcal{S}_{++}^n$, as tangent classifiers. This section systematically studies all Riemannian logarithmic maps between \mathcal{S}_{++}^n and $T_I \mathcal{S}_{++}^n$, under seven families of metrics.

4.1 RIEMANNIAN LOGARITHMS UNDER SEVEN DEFORMED METRICS

Table 2: Log_I under seven families of metrics. $\theta_0 = \frac{\theta_1 + \theta_2}{2}$ for (θ_1, θ_2) -EM, $\theta_0 = \theta$ for (θ, α, β) -EM and 2θ -BWM, and $(2\theta, \phi_{2\theta}(P))$ -BWM.

Metric	$\text{Log}_I P$	Metric	$\text{Log}_I P$
(α, β) -LEM	mlog(P)	(θ, α, β) -EM	$\frac{1}{\theta_0}(P^{\theta_0} - I)$
(θ, α, β) -AIM		(θ_1, θ_2) -EM	
θ -LCM	$\frac{1}{\theta} \left[[\tilde{L}] + [\tilde{L}]^\top + 2 \text{Dlog}(\mathbb{D}(\tilde{L})) \right]$	2θ -BWM	
		$(2\theta, P^{2\theta})$ -BWM	

The matrix logarithm is generally characterized as the Riemannian logarithm Log_I at I under the standard LEM and AIM. Inspired by this, we systematically investigate Riemannian logarithms on SPD manifolds. Let P denote an SPD matrix and \tilde{L} represent the Cholesky factor of P^θ . Tab. 2 presents the Riemannian logarithms at I under all seven metrics, where $[\cdot]$ is the strictly lower triangular part of a square matrix, $\mathbb{D}(\cdot)$ is a diagonal matrix, and $\text{Dlog}(\cdot)$ is the diagonal logarithm. We leave technical details in App. E.

Remark 1. Let us elaborate further on the parameter of GBWM in Tab. 2. Given an SPD point $P \in \mathcal{S}_{++}^n$, P -BWM coincides with the standard AIM in the neighborhood of P (Han et al., 2021). This local property could be beneficial (Han et al., 2023). Similarly, $(2\theta, P^{2\theta})$ -BWM is locally $(2\theta, 1, 0)$ -AIM, the deformed metric of the standard AIM. Please refer to App. F for technical details.

Tab. 2 implies that there are three types of Log_I :

$$\text{Matrix-logarithm-based: } \text{mlog}(P), \quad (6)$$

$$\text{Matrix-power-based: } \frac{1}{\theta}(P^\theta - I), \quad (7)$$

$$\text{LCM-based: } \frac{1}{\theta} \left[[\tilde{L}] + [\tilde{L}]^\top + 2 \text{Dlog}(\mathbb{D}(\tilde{L})) \right], \quad (8)$$

We denote the tangent MLR induced by Eq. (6), *i.e.*, Eq. (6) + vectorization + FC + softmax, as Log-TMLR, while the counterparts of Eq. (7) and Eq. (8) is referred to as Pow-TMLR and Cho-TMLR, respectively. Obviously, Log-TMLR is the exact Log-EMLR (Eq. (4)) used in GCP.

Table 3: Results of GCP on the ImageNet-1k and Cars datasets with Pow-TMLR or Pow-EMLR under the architecture of ResNet-18.

Method	ImageNet-1k		Cars	
	Top-1 Acc (%)	Top-5 Acc (%)	Top-1 Acc (%)	Top-5 Acc (%)
Pow-TMLR	71.62	89.73	51.14	74.29
Pow-EMLR	73	90.91	80.43	94.15

4.2 POW-TMLR VERSUS POW-EMLR

Pow-EMLR applies Euclidean MLR directly on the non-Euclidean SPD manifold, while Pow-TMLR applies Euclidean MLR on the Euclidean space of $T_I \mathcal{S}_{++}^n$. *In this sense, Pow-TMLR should be more theoretically advantageous than Pow-EMLR.* Moreover, the difference between Pow-EMLR and Pow-TMLR seems to be minor. Pow-EMLR differs from Pow-TMLR only in a simple affine transformation $f_\theta(X) = \frac{1}{\theta}(X - I)$. Note that the composition of affine transformations remains affine, and the FC layer is also an affine transformation. Therefore, Pow-EMLR might be viewed as the approximation of Pow-TMLR. **Based on this discussion, we hypothesize that the tangent classifier serves as the underlying mechanism of matrix functions in GCP.** If this hypothesis holds, Pow-EMLR should perform worse or at least similarly to Pow-TMLR.

To validate this postulation, we conduct experiments on the ImageNet-1k (Deng et al., 2009) and Stanford Cars (Cars) (Krause et al., 2013) datasets. We use the architecture of ResNet-18 and ResNet-50 (He et al., 2016) on the ImageNet and Cars datasets, respectively. Following the classic iSQRT-COV (Li et al., 2018), we set $\text{power}=1/2$ and use Newton-Schulz iteration to calculate the matrix square root. Note that Pow-EMLR under Newton-Schulz iteration is exactly the original implementation of iSQRT-COV. As shown in Tab. 3, opposite to our hypothesis, Pow-TMLR is inferior to Pow-EMLR for classifying covariance matrices in GCP. Similar trends are also observed in additional experiments conducted on FGVC datasets, as will be presented in Sec. 6. **These findings suggest that instead of tangent classifiers, there should exist other more fundamental mechanisms for underpinning matrix functions in GCP.**

5 MATRIX FUNCTIONS AND RIEMANNIAN CLASSIFIERS

Recently, Riemannian classifiers on the SPD manifold, which can more faithfully respect the innate geometry, have exhibited more promising performance than tangent classifiers (Nguyen & Yang,

270 2023; Chen et al., 2024a;c). This section will demonstrate that matrix functions in GCP implicitly
 271 respect Riemannian classifiers, which offers a unified theoretical explanation of the working mech-
 272 anism of matrix functions. We start with reviewing the Riemannian SPD classifiers and then present
 273 our theoretical analysis in detail.

275 5.1 SPD MULTINOMIAL LOGISTICS REGRESSION REVISITED

276 Inspired by (Lebanon & Lafferty, 2004; Ganea et al., 2018), some recent works (Nguyen & Yang,
 277 2023; Chen et al., 2024a;c) extended the Euclidean MLR into SPD manifolds. We first revisit the
 278 reformulation of the Euclidean MLR, and then move on to the SPD MLRs introduced in (Chen et al.,
 279 2024c), especially the ones induced by (θ, α, β) -EM and (α, β) -LEM.

281 The Euclidean MLR calculates the probability of each class by

$$282 \quad \forall k \in \{1, \dots, C\}, \quad p(y = k | x) \propto \exp(\langle a_k, x \rangle - b_k), \quad (9)$$

284 where $x \in \mathbb{R}^n$ is an input vector, C is the number of classes, $b_k \in \mathbb{R}$, and $a_k \in \mathbb{R}^n \setminus \{0\}$. Eq. (9)
 285 can be further rewritten as

$$286 \quad p(y = k | x) \propto \exp(\langle a_k, x - p_k \rangle), \quad (10)$$

287 where p_k satisfies $\langle a_k, p_k \rangle = b_k$. As shown in the previous literature (Lebanon & Lafferty, 2004;
 288 Ganea et al., 2018), Eq. (10) can be further reformulated by the margin distance to the hyperplane:

$$290 \quad p(y = k | x) \propto \exp(\text{sign}(\langle a_k, x - p_k \rangle) \|a_k\| d(x, H_{a_k, p_k})), \quad (11)$$

291 where $p_k \in \mathbb{R}^n$ satisfying $\langle a_k, p_k \rangle = b_k$, and the hyperplane H_{a_k, p_k} is defined as:

$$292 \quad H_{a_k, p_k} = \{x \in \mathbb{R}^n : \langle a_k, x - p_k \rangle = 0\}. \quad (12)$$

293 Chen et al. (2024c) generalized Eqs. (11) and (12) into general manifolds and proposed the SPD
 294 MLRs under five families of metrics. The SPD MLRs under (α, β) -LEM and (θ, α, β) -EM are

$$297 \quad (\alpha, \beta)\text{-LEM-based: } p(y = k | S) \propto \exp[\langle \log(S) - \log(P_k), A_k \rangle^{(\alpha, \beta)}], \quad (13)$$

$$299 \quad (\theta, \alpha, \beta)\text{-EM-based: } p(y = k | S) \propto \exp\left[\frac{1}{\theta} \langle S^\theta - P_k^\theta, A_k \rangle^{(\alpha, \beta)}\right], \quad (14)$$

301 where $\alpha > 0$, $\beta > -\alpha/n$, and S is an input SPD feature. Here, $P_k \in \mathcal{S}_{++}^n$ and $A_k \in T_I \mathcal{S}_{++}^n \cong \mathcal{S}^n$
 302 are parameters for each class k . In Eqs. (13) and (14), the formula within $\exp(\cdot)$ can be viewed as
 303 the counterpart of the Euclidean FC layer in SPD manifolds, extracting features to calculate softmax
 304 probabilities.

306 5.2 MATRIX FUNCTIONS AS SPD MULTINOMIAL LOGISTICS REGRESSION

307 Under the standard LEM ((1, 0)-LEM) and PEM (($\theta, 1, 0$)-EM), Eqs. (13) and (14) become

$$308 \quad \text{LEM-based: } \exp[\langle \log(S) - \log(P_k), A_k \rangle], \quad (15)$$

$$310 \quad \text{PEM-based: } \exp\left[\frac{1}{\theta} \langle S^\theta - P_k^\theta, A_k \rangle\right], \quad (16)$$

311 Eqs. (15) and (16) appear to be far away from the Log-/Pow-EMLR in GCP, as the SPD parameters
 312 $\{P_{1..C}\}$ requires Riemannian optimization. However, Chen et al. (2024a, Prop. 5.1) show that
 313 under the LEM-based Riemannian Stochastic Gradient Descent (RSGD) for each P_k and Euclidean
 314 SGD for each A_k , Eq. (15) is equivalent to a Euclidean MLR optimized by the Euclidean SGD in
 315 the co-domain of the matrix logarithm. Similar to LEM, we have the following proposition w.r.t.
 316 PEM.

317 **Theorem 2.** [\downarrow] Under PEM with $\theta > 0$, optimizing each SPD parameter P_k in Eq. (16) by PEM-
 318 based RSGD and Euclidean parameter A_k by Euclidean SGD, the PEM-based SPD MLR is equiv-
 319 alent to a Euclidean MLR illustrated in Eq. (10) in the co-domain of $\phi_\theta(\cdot) : \mathcal{S}_{++}^n \rightarrow \mathcal{S}_{++}^n$, defined
 320 as

$$322 \quad \phi_\theta(S) = \frac{1}{\theta} S^\theta, \theta > 0, \forall S \in \mathcal{S}_{++}^n. \quad (17)$$

Table 4: Intrinsic explanations of some classifiers for GCP. For Cho-TMLR, $\tilde{L} = \text{Chol}(S^\theta)$. For Pow-TMLR, $\theta_0 = \frac{\theta_1 + \theta_2}{2}$ for (θ_1, θ_2) -EM, $\theta_0 = \theta$ for (θ, α, β) -EM, $\theta_0 = 2\theta$ for 2θ -BWM and $(2\theta, \phi_{2\theta}(S))$ -BWM. Here, $f_s(\cdot)$ denotes the softmax, $\mathcal{F}(\cdot)$ denotes the FC layer, and $\tilde{V} = \frac{1}{\theta} \left[[\tilde{L}] + [\tilde{L}]^\top + 2 \text{Dlog}(\mathbb{D}(\tilde{L})) \right]$ with $S^\theta = \tilde{L}\tilde{L}^\top$ as the Cholesky decomposition.

	Log-EMLR	Pow-EMLR	ScalePow-EMLR	Pow-TMLR	Cho-TMLR
Expression	$f_s(\mathcal{F}(f_{\text{vec}}(\text{mlog}(S))))$	$f_s(\mathcal{F}(f_{\text{vec}}(S^\theta)))$ ($\theta > 0$)	$f_s(\mathcal{F}(f_{\text{vec}}(\frac{1}{\theta}S^\theta)))$ ($\theta > 0$)	$f_s(\mathcal{F}(f_{\text{vec}}(\frac{1}{\theta_0}(S^{\theta_0} - I))))$	$f_s(\mathcal{F}(f_{\text{vec}}(\tilde{V})))$
Explanation	SPD MLR	SPD MLR	SPD MLR	Tangent Classifier	Tangent Classifier
Metrics	LEM	$(\theta, 1, 0)$ -EM	$(\theta, 1, 0)$ -EM	(θ, α, β) -EM, (θ_1, θ_2) -EM, 2θ -BWM, $(2\theta, \phi_{2\theta}(S))$ -BWM	θ -LCM
Used in GCP	✓(Eq. (4))	✓ ($\theta = 0.5$ in Eq. (5))	✗	✗	✗
Reference	(Chen et al., 2024a, Prop. 5.1)	Thm. 2	Thm. 2	Tab. 2	Tab. 2

We define ScalePow-EMLR as $\text{softmax}(\mathcal{F}(f_{\text{vec}}(\frac{1}{\theta}S^\theta); A, b))$. Then, ScalePow-EMLR respects the SPD MLR under the standard PEM. The only difference between ScalePow-EMLR and Pow-EMLR (Eq. (5)) is the scalar product before vectorization, which is expected to have minor effects on DNNs. Obviously, we have

$$\mathcal{F}\left(f_{\text{vec}}\left(\frac{1}{\theta}S^\theta\right); A, b\right) = \mathcal{F}\left(f_{\text{vec}}(S^\theta); \tilde{A}, b\right). \quad (18)$$

where $\tilde{A} = \frac{1}{\theta}A$. Therefore, from a forward perspective, ScalePow-EMLR is equivalent to the original Pow-EMLR. Besides, by scaled initialization and learning rate of A , ScalePow-EMLR could be completely equivalent to Pow-EMLR during network training. Note that this analysis cannot be transferred into Pow-TMLR. Please refer to App. G for more details.

Therefore, the Pow-EMLR in GCP is implicitly an SPD MLR induced by $(\theta, 1, 0)$ -EM. For the widely used matrix square root normalization, it respects the SPD MLR induced by $(1/2, 1, 0)$ -EM. We summarize all the findings in Tab. 4. Besides, Thm. 2 can be easily extended into the case of $\theta < 0$. In this case, our work can also offer theoretical insights for the inverse of covariance ($\theta = -1$) proposed by Rahman et al. (2023). More details are presented in App. J.

5.3 THEORETICAL INSIGHTS ON THE MATRIX POWER AND LOGARITHM

Previous studies on GCP (Li et al., 2017; Wang et al., 2020a; Song et al., 2021) have *empirically* demonstrated a clear advantage of the matrix power (particularly matrix square root) over matrix logarithm. This subsection offers novel theoretical insights to disentangle the different performance between the matrix logarithm and power in GCP.

As shown by Tab. 4, both matrix logarithm and matrix power implicitly build SPD MLRs. However, the Riemannian metrics they respect are different. Matrix power respects $(\theta, 1, 0)$ -EM, while matrix logarithm respects LEM. Both $(\theta, 1, 0)$ -EM and LEM share $O(n)$ -invariance (Chen et al., 2024c), a powerful property in characterizing covariance matrices. Besides, $(\theta, 1, 0)$ -EM is a deformed metric of LEM, interpolating between the standard EM ($\theta = 1$) and LEM ($\theta \rightarrow 0$) (Thanwerdas & Pennec, 2022). The standard EM might suffer from a swelling effect for characterizing SPD matrices (Arsigny et al., 2005), while LEM might over-stretch the eigenvalues of SPD matrices due to the computation of matrix logarithm (Song et al., 2021). Consequently, $(\theta, 1, 0)$ -EM represents balanced alternatives between the standard LEM and EM. In addition, as shown by Chen et al. (2024c, Tab. 4), $(\theta, 1, 0)$ -EM could perform better than LEM regarding SPD MLR. Therefore, the empirical advantages of matrix power over matrix logarithm in the GCP could be attributed to the characteristics of the underlying Riemannian metrics.

6 EXPERIMENTS

In this section, we validate the following hypothesis based on our previous theoretical analysis.

(A1) As Pow-EMLR approximates the tangent classifier Pow-TMLR, the working mechanism of Pow-EMLR is attributed to the **tangent classifier**;

Table 5: Results of iSQRT-COV on four datasets with different covariance matrix classifiers. The backbone network on ImageNet is ResNet-18, while the one on the other three FGVC datasets is ResNet-50. Power is set to be $1/2$ for Pow-TMLR, ScalePow-EMLR and Pow-EMLR.

Classifier	ImageNet-1k		Aircrafts		Birds		Cars	
	Top-1 Acc (%)	Top-5 Acc (%)	Top-1 Acc (%)	Top-5 Acc (%)	Top-1 Acc (%)	Top-5 Acc (%)	Top-1 Acc (%)	Top-5 Acc (%)
Cho-TMLR	N/A	N/A	78.97	91.81	48.07	72.59	51.06	74.33
Pow-TMLR	71.62	89.73	69.58	88.68	52.97	77.80	51.14	74.29
ScalePow-EMLR	72.43	90.44	71.05	89.86	63.48	84.69	80.31	94.07
Pow-EMLR	73	90.91	72.07	89.83	63.29	84.66	80.43	94.15

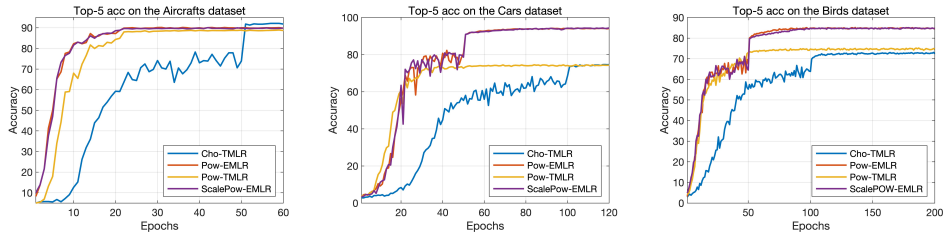


Figure 3: The validation top-5 accuracy on the three FGVC datasets for iSQRT-COV with different classifiers using the ResNet-50 backbone.

(A2) As both Pow-EMLR and Log-EMLR in GCP are equivalent to Riemannian classifiers, the mechanism of matrix normalization should be attributed to **Riemannian classifiers**.

We implement different classifiers for covariance matrix classification, including the original Pow-EMLR, the tangent classifiers Pow-TMLR and Cho-TMLR, and the intrinsic ScalePow-EMLR. We use the Caltech University Birds (Birds) (Welinder et al., 2010), FGVC Aircrafts (Aircrafts) (Maji et al., 2013), Stanford Cars (Cars) (Krause et al., 2013), and ImageNet-1k (Deng et al., 2009) datasets. As the matrix square root is the most effective matrix function in GCP, we set power = $1/2$. In all experiments, we train the network from scratch. More implementation details are in App. H.

6.1 MAIN RESULTS

Notably, although ScalePow-EMLR is equivalent to Pow-EMLR under scaled settings, we implement them under the same network settings for a complete comparison. The results on four datasets are shown in Tab. 5. Our main empirical observations are as follows:

- (1). **Pow-EMLR > Pow-TMLR.** Pow-EMLR generally outperforms Pow-TMLR, especially on Cars and Birds datasets. Recalling in Tab. 4, the expression of Pow-EMLR differs from Pow-TMLR only in an affine transformation. However, across all four datasets, Pow-EMLR consistently surpasses Pow-TMLR. On the Birds and Cars datasets, Pow-EMLR outperforms Pow-TMLR by a large margin. For example, on the Birds dataset, the top-5 accuracy of Pow-EMLR and Pow-TMLR is 84.66% and 77.80%, respectively, whereas, on the Cars dataset, it is 94.15% and 74.29%.
- (2). **Pow-EMLR ≈ ScalePow-EMLR.** Pow-EMLR shows comparable performance to ScalePow-EMLR. Recalling in Tab. 4, the only difference between Pow-EMLR and ScalePow-EMLR is a scalar product. Moreover, as discussed in Sec. 5.2 this minor difference can be further solved by scaled initialization of the FC layer. Although we use the same initialization for a fair comparison, Pow-EMLR and ScalePow-EMLR show similar performance.
- (3). **Pow-EMLR ≫ Cho-TMLR.** While Cho-TMLR demonstrates the best performance on the Aircrafts datasets, it exhibits the worst performance on the other two FGVC datasets. On the Cars and Birds datasets, Pow-EMLR surpasses Cho-TMLR by a large margin. The unstable performance of Cho-TMLR might be attributed to the diagonal logarithm, which might overly stretch the diagonal elements of the Cholesky factor.

Based on the above empirical findings, we can reach the following conclusion. (A1) is **refuted** by (1). The inferior performance of Pow-TMLR against Pow-EMLR in (1) indicates that Pow-EMLR can not be simply viewed as equivalent to the tangent classifier Pow-TMLR. (A2) is **validated** by (2). (2) validates our theoretical postulation that the effectiveness of matrix power should be attributed to the Riemannian classifier it implicitly constructs.

Other findings. In the first and last observations, tangent classifiers are less effective than the Riemannian classifier. Tangent classifiers can distort the innate geometry of the manifold, as the tangent space is only a local linear approximation of the manifold. In contrast, the Riemannian classifier can faithfully respect the geometry of the manifold. Besides, although Log-EMLR coincides with both tangent and Riemannian classifiers, the real underlying mechanism of matrix logarithm should also be attributed to the Riemannian classifier instead of the tangent classifier.

Table 6: Ablations of Pow-EMLR, ScalePow-EMLR, and Pow-TMLR under different settings.

(a) Results of different powers under the ResNet-50.

Classifier	Aircrafts		Cars	
	Top-1 Acc (%)	Top-5 Acc (%)	Top-1 Acc (%)	Top-5 Acc (%)
Pow-TMLR-0.25	65.41	86.71	41.47	66.66
ScalePow-EMLR-0.25	72.76	90.31	61.78	84.04
Pow-EMLR-0.25	71.47	90.04	62.88	84.14
Pow-TMLR-0.5	67.9	88.75	55.01	77.95
ScalePow-EMLR-0.5	74.29	91.12	62.42	84.82
Pow-EMLR-0.5	74.17	91.21	62.83	84.85
Pow-TMLR-0.7	65.92	87.49	50.68	74.12
ScalePow-EMLR-0.7	74.26	91.15	64.22	83.67
Pow-EMLR-0.7	74.17	90.49	61.41	82.39

(b) Results under the AlexNet.

Dataset	Result	Pow-TMLR	Pow-EMLR
Aircrafts	Top-1 Acc (%)	38.01	65.02
	Top-5 Acc (%)	74.4	87.79
Cars	Top-1 Acc (%)	28.57	59.13
	Top-5 Acc (%)	59.51	82.04

6.2 TRAINING DYNAMICS AND ABLATIONS

Training dynamics. Fig. 3 presents the top-5 validation accuracy curves on three FGVC datasets. Pow-EMLR exhibits comparable performance to ScalePow-EMLR throughout the training. Moreover, Pow-EMLR consistently outperforms Pow-TMLR, particularly on the Cars and Birds datasets. This again suggests that the effectiveness of Pow-EMLR should be attributed to the Riemannian MLR rather than the tangent classifier. Furthermore, we note that the decreasing learning rate plays a crucial role in Cho-TMLR. On the Aircrafts dataset, before the 50th epoch, Cho-TMLR exhibits the worst performance among all classifiers. However, after the 50th epoch, when the learning rate reduces, Cho-TMLR surpasses all the other classifiers. Nonetheless, on the remaining two datasets, Cho-TMLR remains inferior throughout the training. This discrepancy may be attributed to the logarithm operation in Cho-TMLR. Recalling Eq. (8), there is a diagonal logarithm for the Cholesky factor. Similar to the matrix logarithm, Eq. (8) will also over-stretch the diagonal elements of the Cholesky factor, compromising the overall performance of Cho-TMLR.

Ablations. To further validate our postulation, we compare Pow-EMLR, SaclePow-EMLR, and Pow-TMLR with different powers under the ResNet-50 architecture, *i.e.*, $\theta = 0.25, 0.5, 0.7$. We also compare Pow-EMLR against Pow-TMLR under the AlexNet architecture. The ablations are conducted on the Aircrafts and Car datasets. The results discussed below confirm again our findings that the mechanism of matrix functions in GCP should be attributed to Riemannian classifiers.

Impact of matrix power. Following Song et al. (2021), we use accurate SVD to calculate the matrix power and Padé approximant for backpropagation. The results are reported in Tab. 6a. Since we use SVD for the matrix power here, the results in Tab. 6a under $\theta = 0.5$ are slightly different from Tab. 5. Nevertheless, Pow-EMLR consistently shows similar performance to ScalePow-EMLR and outperforms Pow-TMLR under different powers.

Impact of architectures. We also use the vanilla AlexNet (Krizhevsky et al., 2012) as an alternative backbone. Tab. 6b presents the comparison results under the AlexNet architecture. Consistent with our previous observation, Pow-EMLR still outperforms Pow-TMLR.

7 CONCLUSIONS AND FUTURE WORK

This paper presents a unified understanding of the role of matrix functions in GCP, including matrix power and logarithm. Our study reveals that matrix functions implicitly construct Riemannian classifiers for classifying covariance matrices, thus justifying the application of the Euclidean classifier after matrix power. We validate our findings through experiments conducted on three FGVC and the large-scale ImageNet datasets. To the best of our knowledge, our work is the **first** to explain the theoretical mechanism behind matrix functions from the perspective of Riemannian geometry. Therefore, our work opens a novel possibility for designing GCP classifiers from a Riemannian perspective. As a future avenue, we will design effective GCP classifiers based on other Riemannian MLRs (Nguyen & Yang, 2023; Chen et al., 2024c).

REFERENCES

- 486
487
488 Dinesh Acharya, Zhiwu Huang, Danda Pani Paudel, and Luc Van Gool. Covariance pooling for
489 facial expression recognition. In *Proceedings of the IEEE Conference on Computer Vision and*
490 *Pattern Recognition Workshops*, pp. 367–374, 2018. URL [https://doi.org/10.1109/](https://doi.org/10.1109/CVPRW.2018.00077)
491 [CVPRW.2018.00077](https://doi.org/10.1109/CVPRW.2018.00077).
- 492 Vincent Arsigny, Pierre Fillard, Xavier Pennec, and Nicholas Ayache. *Fast and simple computations*
493 *on tensors with log-Euclidean metrics*. PhD thesis, INRIA, 2005. URL [https://doi.org/](https://doi.org/10.1007/11566465_15)
494 [10.1007/11566465_15](https://doi.org/10.1007/11566465_15).
- 495
496 Rajendra Bhatia. *Positive Definite Matrices*. Princeton University Press, 2009. URL [https://doi.org/](https://doi.org/10.1515/9781400827787)
497 [10.1515/9781400827787](https://doi.org/10.1515/9781400827787).
- 498 Rajendra Bhatia, Tanvi Jain, and Yongdo Lim. On the Bures-Wasserstein distance between positive
499 definite matrices. *Expositiones Mathematicae*, 37(2):165–191, 2019. URL [https://doi.](https://doi.org/10.1016/j.exmath.2018.01.002)
500 [org/10.1016/j.exmath.2018.01.002](https://doi.org/10.1016/j.exmath.2018.01.002).
- 501
502 Silvere Bonnabel. Stochastic gradient descent on Riemannian manifolds. *IEEE Transactions on Au-*
503 *tomatic Control*, 58(9):2217–2229, 2013. URL [https://doi.org/10.1109/TAC.2013.](https://doi.org/10.1109/TAC.2013.2254619)
504 [2254619](https://doi.org/10.1109/TAC.2013.2254619).
- 505 Ziheng Chen, Tianyang Xu, Xiao-Jun Wu, Rui Wang, Zhiwu Huang, and Josef Kittler. Riemannian
506 local mechanism for SPD neural networks. In *Proceedings of the AAAI Conference on*
507 *Artificial Intelligence*, pp. 7104–7112, 2023. URL [https://doi.org/10.1609/aaai.](https://doi.org/10.1609/aaai.v37i6.25867)
508 [v37i6.25867](https://doi.org/10.1609/aaai.v37i6.25867).
- 509
510 Ziheng Chen, Yue Song, Gaowen Liu, Ramana Rao Kompella, Xiao-Jun Wu, and Nicu Sebe.
511 Riemannian multinomial logistics regression for SPD neural networks. In *Proceedings of*
512 *the IEEE/CVF Conference on Computer Vision and Pattern Recognition*, pp. 17086–17096,
513 2024a. URL [https://openaccess.thecvf.com/content/CVPR2024/html/](https://openaccess.thecvf.com/content/CVPR2024/html/Chen_Riemannian_Multinomial_Logistics_Regression_for_SPD_Neural_Networks_CVPR_2024_paper.html)
514 [Chen_Riemannian_Multinomial_Logistics_Regression_for_SPD_Neural_](https://openaccess.thecvf.com/content/CVPR2024/html/Chen_Riemannian_Multinomial_Logistics_Regression_for_SPD_Neural_Networks_CVPR_2024_paper.html)
515 [Networks_CVPR_2024_paper.html](https://openaccess.thecvf.com/content/CVPR2024/html/Chen_Riemannian_Multinomial_Logistics_Regression_for_SPD_Neural_Networks_CVPR_2024_paper.html).
- 516 Ziheng Chen, Yue Song, Yunmei Liu, and Nicu Sebe. A Lie group approach to Riemannian normal-
517 ization for SPD neural networks. In *The Twelfth International Conference on Learning Representations*,
518 2024b. URL <https://openreview.net/forum?id=okYdj8Ysru>.
- 519
520 Ziheng Chen, Yue Song, Xiaojun, and Nicu Sebe. RMLR: Extending multinomial logistic regression
521 into general geometries. In *Advances in Neural Information Processing Systems*, 2024c. URL
522 <https://arxiv.org/abs/2409.19433>.
- 523
524 Ziheng Chen, Yue Song, Tianyang Xu, Zhiwu Huang, Xiao-Jun Wu, and Nicu Sebe. Adaptive
525 log-Euclidean metrics for SPD matrix learning. *IEEE Transactions on Image Processing*, 2024d.
526 URL <https://doi.org/10.1109/TIP.2024.3451930>.
- 527
528 Yin Cui, Feng Zhou, Jiang Wang, Xiao Liu, Yuanqing Lin, and Serge Belongie. Kernel pooling
529 for convolutional neural networks. In *Proceedings of the IEEE Conference on Computer Vision*
530 *and Pattern Recognition*, pp. 2921–2930, 2017. URL [https://doi.org/10.1109/CVPR.](https://doi.org/10.1109/CVPR.2017.325)
531 [2017.325](https://doi.org/10.1109/CVPR.2017.325).
- 532
533 Jia Deng, Wei Dong, Richard Socher, Li-Jia Li, Kai Li, and Li Fei-Fei. ImageNet: A large-scale hier-
534 archical image database. In *2009 IEEE Conference on Computer Vision and Pattern Recognition*,
535 pp. 248–255. IEEE, 2009. URL <https://doi.org/10.1109/CVPR.2009.5206848>.
- 536
537 Ian L Dryden, Xavier Pennec, and Jean-Marc Peyrat. Power Euclidean metrics for covariance ma-
538 trices with application to diffusion tensor imaging. *arXiv preprint arXiv:1009.3045*, 2010. URL
539 <https://arxiv.org/abs/1009.3045>.
- 538
539 Octavian Ganea, Gary Bécigneul, and Thomas Hofmann. Hyperbolic neural networks. *Advances in*
Neural Information Processing Systems, 31, 2018. URL [https://dl.acm.org/doi/10.](https://dl.acm.org/doi/10.5555/3327345.3327440)
[5555/3327345.3327440](https://dl.acm.org/doi/10.5555/3327345.3327440).

- 540 Yang Gao, Oscar Beijbom, Ning Zhang, and Trevor Darrell. Compact bilinear pooling. In *Proceed-*
541 *ings of the IEEE Conference on Computer Vision and Pattern Recognition*, pp. 317–326, 2016.
542 URL <https://doi.org/10.1109/CVPR.2016.41>.
- 543
- 544 Andi Han, Bamdev Mishra, Pratik Kumar Jawanpuria, and Junbin Gao. On Riemannian optimiza-
545 tion over positive definite matrices with the Bures-Wasserstein geometry. *Advances in Neural*
546 *Information Processing Systems*, 34:8940–8953, 2021. URL [https://openreview.net/](https://openreview.net/forum?id=ZCHxGFmc62a)
547 [forum?id=ZCHxGFmc62a](https://openreview.net/forum?id=ZCHxGFmc62a).
- 548 Andi Han, Bamdev Mishra, Pratik Jawanpuria, and Junbin Gao. Learning with symmetric positive
549 definite matrices via generalized Bures-Wasserstein geometry. In *International Conference on*
550 *Geometric Science of Information*, pp. 405–415. Springer, 2023. URL [https://doi.org/](https://doi.org/10.1007/978-3-031-38271-0_40)
551 [10.1007/978-3-031-38271-0_40](https://doi.org/10.1007/978-3-031-38271-0_40).
- 552
- 553 Kaiming He, Xiangyu Zhang, Shaoqing Ren, and Jian Sun. Deep residual learning for image recog-
554 nition. In *Proceedings of the IEEE Conference on Computer Vision and Pattern Recognition*, pp.
555 770–778, 2016. URL <https://doi.org/10.1109/CVPR.2016.90>.
- 556 Catalin Ionescu, Orestis Vantzos, and Cristian Sminchisescu. Matrix backpropagation for deep net-
557 works with structured layers. In *Proceedings of the IEEE International Conference on Computer*
558 *Vision*, pp. 2965–2973, 2015. URL <https://doi.org/10.1109/ICCV.2015.339>.
- 559
- 560 Shu Kong and Charless Fowlkes. Low-rank bilinear pooling for fine-grained classification. In
561 *Proceedings of the IEEE Conference on Computer Vision and Pattern Recognition*, pp. 365–374,
562 2017. URL <https://doi.org/10.1109/CVPR.2017.743>.
- 563 Piotr Koniusz, Fei Yan, Philippe-Henri Gosselin, and Krystian Mikolajczyk. Higher-order occur-
564 rence pooling for bags-of-words: Visual concept detection. *IEEE Transactions on Pattern Anal-*
565 *ysis and Machine Intelligence*, 39(2):313–326, 2017. URL [https://doi.org/10.1109/](https://doi.org/10.1109/TPAMI.2016.2545667)
566 [TPAMI.2016.2545667](https://doi.org/10.1109/TPAMI.2016.2545667).
- 567 Piotr Koniusz, Lei Wang, and Anoop Cherian. Tensor representations for action recognition. *IEEE*
568 *Transactions on Pattern Analysis and Machine Intelligence*, 44(2):648–665, 2021. URL [https://doi.org/](https://doi.org/10.1109/TPAMI.2021.3107160)
569 [10.1109/TPAMI.2021.3107160](https://doi.org/10.1109/TPAMI.2021.3107160).
- 570
- 571 Jonathan Krause, Michael Stark, Jia Deng, and Li Fei-Fei. 3D object representations for fine-
572 grained categorization. In *Proceedings of the IEEE International Conference on Computer Vision*
573 *Workshops*, pp. 554–561, 2013. URL <https://doi.org/10.1109/ICCVW.2013.77>.
- 574
- 575 Alex Krizhevsky, Ilya Sutskever, and Geoffrey E Hinton. Imagenet classification with deep convo-
576 lutional neural networks. *Advances in Neural Information Processing Systems*, 25, 2012. URL
577 <https://doi.org/10.1145/3065386>.
- 578 Guy Lebanon and John Lafferty. Hyperplane margin classifiers on the multinomial manifold. In
579 *Proceedings of the twenty-first international conference on Machine learning*, pp. 66, 2004. URL
580 <https://doi.org/10.1145/1015330.1015333>.
- 581
- 582 Peihua Li, Jiangtao Xie, Qilong Wang, and Wangmeng Zuo. Is second-order information helpful for
583 large-scale visual recognition? In *Proceedings of the IEEE International Conference on Computer*
584 *Vision*, pp. 2070–2078, 2017. URL <https://doi.org/10.1109/ICCV.2017.228>.
- 585
- 586 Peihua Li, Jiangtao Xie, Qilong Wang, and Zilin Gao. Towards faster training of global covariance
587 pooling networks by iterative matrix square root normalization. In *Proceedings of the IEEE*
588 *Conference on Computer Vision and Pattern Recognition*, pp. 947–955, 2018. URL [https://doi.org/](https://doi.org/10.1109/CVPR.2018.00105)
[10.1109/CVPR.2018.00105](https://doi.org/10.1109/CVPR.2018.00105).
- 589
- 590 Tsung-Yu Lin and Subhransu Maji. Improved bilinear pooling with CNNs. *arXiv preprint*
591 *arXiv:1707.06772*, 2017. URL <https://arxiv.org/abs/1707.06772>.
- 592
- 593 Tsung-Yu Lin, Aruni RoyChowdhury, and Subhransu Maji. Bilinear CNN models for fine-grained
visual recognition. In *Proceedings of the IEEE International Conference on Computer Vision*, pp.
1449–1457, 2015. URL <https://doi.org/10.1109/ICCV.2015.170>.

- 594 Tsung-Yu Lin, Subhransu Maji, and Piotr Koniusz. Second-order democratic aggregation. In *Proceedings of the European Conference on Computer Vision (ECCV)*, pp. 620–636, 2018. URL https://doi.org/10.1007/978-3-030-01219-9_38.
- 595
- 596
- 597 Zhenhua Lin. Riemannian geometry of symmetric positive definite matrices via Cholesky decomposition. *SIAM Journal on Matrix Analysis and Applications*, 40(4):1353–1370, 2019. URL <https://doi.org/10.1137/18M1221084>.
- 598
- 599
- 600
- 601 Hanxiao Liu, Karen Simonyan, and Yiming Yang. DARTS: Differentiable architecture search. In *International Conference on Learning Representations*, 2019. URL <https://openreview.net/forum?id=S1eYHoC5FX>.
- 602
- 603
- 604 Ze Liu, Yutong Lin, Yue Cao, Han Hu, Yixuan Wei, Zheng Zhang, Stephen Lin, and Baining Guo. Swin transformer: Hierarchical vision transformer using shifted windows. In *Proceedings of the IEEE/CVF International Conference on Computer Vision*, pp. 10012–10022, 2021. URL <https://doi.org/10.1109/ICCV48922.2021.00986>.
- 605
- 606
- 607
- 608 Subhransu Maji, Esa Rahtu, Juho Kannala, Matthew Blaschko, and Andrea Vedaldi. Fine-grained visual classification of aircraft. *arXiv preprint arXiv:1306.5151*, 2013. URL <https://arxiv.org/abs/1306.5151>.
- 609
- 610
- 611
- 612 Xuan Son Nguyen. Geomnet: A neural network based on Riemannian geometries of SPD matrix space and Cholesky space for 3D skeleton-based interaction recognition. In *Proceedings of the IEEE International Conference on Computer Vision*, pp. 13379–13389, 2021. URL <https://doi.org/10.1109/ICCV48922.2021.01313>.
- 613
- 614
- 615
- 616 Xuan Son Nguyen. The Gyro-structure of some matrix manifolds. In *Advances in Neural Information Processing Systems*, volume 35, pp. 26618–26630, 2022a. URL https://proceedings.neurips.cc/paper_files/paper/2022/file/a9ad92a81748a31ef6f2ef68d775da46-Paper-Conference.pdf.
- 617
- 618
- 619
- 620 Xuan Son Nguyen. A Gyrovector space approach for symmetric positive semi-definite matrix learning. In *Proceedings of the European Conference on Computer Vision*, pp. 52–68, 2022b. URL https://doi.org/10.1007/978-3-031-19812-0_4.
- 621
- 622
- 623
- 624 Xuan Son Nguyen and Shuo Yang. Building neural networks on matrix manifolds: A Gyrovector space approach. *arXiv preprint arXiv:2305.04560*, 2023. URL <https://dl.acm.org/doi/10.5555/3618408.3619491>.
- 625
- 626
- 627 Xavier Pennec, Pierre Fillard, and Nicholas Ayache. A Riemannian framework for tensor computing. *International Journal of Computer Vision*, 66(1):41–66, 2006. URL <https://doi.org/10.1007/s11263-005-3222-z>.
- 628
- 629
- 630
- 631 Saimunur Rahman, Lei Wang, Changming Sun, and Luping Zhou. Redro: Efficiently learning large-sized SPD visual representation. In *European Conference on Computer Vision*, pp. 1–17. Springer, 2020. URL https://doi.org/10.1007/978-3-030-58555-6_1.
- 632
- 633
- 634 Saimunur Rahman, Piotr Koniusz, Lei Wang, Luping Zhou, Peyman Moghadam, and Changming Sun. Learning partial correlation based deep visual representation for image classification. In *Proceedings of the IEEE/CVF Conference on Computer Vision and Pattern Recognition*, pp. 6231–6240, 2023. URL <https://doi.org/10.1109/CVPR52729.2023.00603>.
- 635
- 636
- 637
- 638 Yue Song, Nicu Sebe, and Wei Wang. Why approximate matrix square root outperforms accurate SVD in global covariance pooling? In *Proceedings of the IEEE International Conference on Computer Vision*, pp. 1115–1123, 2021. URL <https://doi.org/10.1109/ICCV48922.2021.00115>.
- 639
- 640
- 641
- 642 Yue Song, Nicu Sebe, and Wei Wang. On the eigenvalues of global covariance pooling for fine-grained visual recognition. *IEEE Transactions on Pattern Analysis and Machine Intelligence*, 45(3):3554–3566, 2022a. URL <https://doi.org/10.1109/TPAMI.2022.3178802>.
- 643
- 644
- 645
- 646 Yue Song, Nicu Sebe, and Wei Wang. Fast differentiable matrix square root and inverse square root. *IEEE Transactions on Pattern Analysis and Machine Intelligence*, 45(6):7367–7380, 2022b. URL <https://doi.org/10.1109/TPAMI.2022.3216339>.
- 647

- 648 Yue Song, Nicu Sebe, and Wei Wang. Fast differentiable matrix square root. In *International Con-*
649 *ference on Learning Representations*, 2022c. URL [https://openreview.net/forum?](https://openreview.net/forum?id=-AOEi-5VTU8)
650 [id=-AOEi-5VTU8](https://openreview.net/forum?id=-AOEi-5VTU8).
- 651 Yue Song, Nicu Sebe, and Wei Wang. Improving covariance conditioning of the svd meta-layer by
652 orthogonality. In *European Conference on Computer Vision*, pp. 356–372. Springer, 2022d. URL
653 https://doi.org/10.1007/978-3-031-20053-3_21.
- 654 Yann Thanwerdas and Xavier Pennec. Exploration of balanced metrics on symmetric positive defi-
655 nite matrices. In *Geometric Science of Information: 4th International Conference, GSI 2019,*
656 *Toulouse, France, August 27–29, 2019, Proceedings 4*, pp. 484–493. Springer, 2019. URL
657 https://doi.org/10.1007/978-3-030-26980-7_50.
- 658 Yann Thanwerdas and Xavier Pennec. The geometry of mixed-Euclidean metrics on symmetric
659 positive definite matrices. *Differential Geometry and its Applications*, 81:101867, 2022. URL
660 <https://doi.org/10.1016/j.difgeo.2022.101867>.
- 661 Yann Thanwerdas and Xavier Pennec. O(n)-invariant Riemannian metrics on SPD matrices. *Linear*
662 *Algebra and its Applications*, 661:163–201, 2023. URL [https://doi.org/10.1016/j.](https://doi.org/10.1016/j.laa.2022.12.009)
663 [laa.2022.12.009](https://doi.org/10.1016/j.laa.2022.12.009).
- 664 Hugo Touvron, Matthieu Cord, Matthijs Douze, Francisco Massa, Alexandre Sablayrolles, and
665 Hervé Jégou. Training data-efficient image transformers & distillation through attention. In
666 *International Conference on Machine Learning*, pp. 10347–10357. PMLR, 2021. URL [https:](https://proceedings.mlr.press/v139/touvron21a.html)
667 [//proceedings.mlr.press/v139/touvron21a.html](https://proceedings.mlr.press/v139/touvron21a.html).
- 668 Qilong Wang, Peihua Li, and Lei Zhang. G2DeNet: Global Gaussian distribution embedding net-
669 work and its application to visual recognition. In *Proceedings of the IEEE Conference on Com-*
670 *puter Vision and Pattern Recognition*, pp. 2730–2739, 2017. URL [https://doi.org/10.](https://doi.org/10.1109/CVPR.2017.689)
671 [1109/CVPR.2017.689](https://doi.org/10.1109/CVPR.2017.689).
- 672 Qilong Wang, Jiangtao Xie, Wangmeng Zuo, Lei Zhang, and Peihua Li. Deep CNNs meet global co-
673 variance pooling: Better representation and generalization. *IEEE Transactions on Pattern Analy-*
674 *sis and Machine Intelligence*, 43(8):2582–2597, 2020a. URL [https://doi.org/10.1109/](https://doi.org/10.1109/TPAMI.2020.2974833)
675 [TPAMI.2020.2974833](https://doi.org/10.1109/TPAMI.2020.2974833).
- 676 Qilong Wang, Li Zhang, Banggu Wu, Dongwei Ren, Peihua Li, Wangmeng Zuo, and Qinghua
677 Hu. What deep CNNs benefit from global covariance pooling: An optimization perspective.
678 In *Proceedings of the IEEE/CVF Conference on Computer Vision and Pattern Recognition*, pp.
679 10771–10780, 2020b. URL <https://doi.org/10.1109/CVPR42600.2020.01078>.
- 680 Qilong Wang, Mingze Gao, Zhaolin Zhang, Jiangtao Xie, Peihua Li, and Qinghua Hu. Dropcov: a
681 simple yet effective method for improving deep architectures. *Advances in Neural Information*
682 *Processing Systems*, 35:33576–33588, 2022a. URL [https://openreview.net/forum?](https://openreview.net/forum?id=QLGuUwDx4S)
683 [id=QLGuUwDx4S](https://openreview.net/forum?id=QLGuUwDx4S).
- 684 Qilong Wang, Zhaolin Zhang, Mingze Gao, Jiangtao Xie, Pengfei Zhu, Peihua Li, Wangmeng Zuo,
685 and Qinghua Hu. Towards a deeper understanding of global covariance pooling in deep learning:
686 An optimization perspective. *IEEE Transactions on Pattern Analysis and Machine Intelligence*,
687 2023. URL <https://10.1109/TPAMI.2023.3321392>.
- 688 Rui Wang, Xiao-Jun Wu, and Josef Kittler. SymNet: A simple symmetric positive definite manifold
689 deep learning method for image set classification. *IEEE Transactions on Neural Networks and*
690 *Learning Systems*, 33(5):2208–2222, 2021. URL [https://doi.org/10.1109/tnnls.](https://doi.org/10.1109/tnnls.2020.3044176)
691 [2020.3044176](https://doi.org/10.1109/tnnls.2020.3044176).
- 692 Rui Wang, Xiao-Jun Wu, Ziheng Chen, Tianyang Xu, and Josef Kittler. DreamNet: A deep
693 Riemannian manifold network for SPD matrix learning. In *Proceedings of the Asian Confer-*
694 *ence on Computer Vision*, pp. 3241–3257, 2022b. URL [https://doi.org/10.1007/](https://doi.org/10.1007/978-3-031-26351-4_39)
695 [978-3-031-26351-4_39](https://doi.org/10.1007/978-3-031-26351-4_39).
- 696 Rui Wang, Xiao-Jun Wu, Ziheng Chen, Tianyang Xu, and Josef Kittler. Learning a discriminative
697 SPD manifold neural network for image set classification. *Neural Networks*, 151:94–110, 2022c.
698 URL <https://doi.org/10.1016/j.neunet.2022.03.012>.
- 699
700
701

- 702 Rui Wang, Xiao-Jun Wu, Ziheng Chen, Cong Hu, and Josef Kittler. SPD manifold deep metric learn-
703 ing for image set classification. *IEEE Transactions on Neural Networks and Learning Systems*,
704 2024. URL <https://doi.org/10.1109/TNNLS.2022.3216811>.
705
- 706 Peter Welinder, Steve Branson, Takeshi Mita, Catherine Wah, Florian Schroff, Serge Belongie, and
707 Pietro Perona. Caltech-UCSD birds 200. 2010. URL [https://www.florian-schroff.](https://www.florian-schroff.de/publications/CUB-200.pdf)
708 [de/publications/CUB-200.pdf](https://www.florian-schroff.de/publications/CUB-200.pdf).
- 709 Jiangtao Xie, Ruiren Zeng, Qilong Wang, Ziqi Zhou, and Peihua Li. Sot: Delving deeper into
710 classification head for transformer. *arXiv preprint arXiv:2104.10935*, 2021. URL [https://](https://arxiv.org/abs/2104.10935)
711 arxiv.org/abs/2104.10935.
- 712 Kaicheng Yu and Mathieu Salzmann. Statistically-motivated second-order pooling. In *Proceedings*
713 *of the European Conference on Computer Vision*, pp. 600–616, 2018. URL [https://doi.](https://doi.org/10.1007/978-3-030-01234-2_37)
714 [org/10.1007/978-3-030-01234-2_37](https://doi.org/10.1007/978-3-030-01234-2_37).
715
- 716 Tan Yu, Yunfeng Cai, and Ping Li. Toward faster and simpler matrix normalization via rank-1
717 update. In *Computer Vision–ECCV 2020: 16th European Conference, Glasgow, UK, August 23–*
718 *28, 2020, Proceedings, Part XIX 16*, pp. 203–219. Springer, 2020. URL [https://doi.org/](https://doi.org/10.1007/978-3-030-58529-7_13)
719 [10.1007/978-3-030-58529-7_13](https://doi.org/10.1007/978-3-030-58529-7_13).
- 720 Li Yuan, Yunpeng Chen, Tao Wang, Weihao Yu, Yujun Shi, Zi-Hang Jiang, Francis EH Tay, Jiashi
721 Feng, and Shuicheng Yan. Tokens-to-token ViT: Training vision transformers from scratch on
722 ImageNet. In *Proceedings of the IEEE/CVF International Conference on Computer Vision*, pp.
723 558–567, 2021. URL <https://doi.org/10.1109/ICCV48922.2021.00060>.
724
- 725 Heliang Zheng, Jianlong Fu, Zheng-Jun Zha, and Jiebo Luo. Learning deep bilinear transformation
726 for fine-grained image representation. *Advances in Neural Information Processing Systems*, 32,
727 2019. URL <https://dl.acm.org/doi/10.5555/3454287.3454672>.
- 728 Pengfei Zhu, Jialu Li, Zhe Dong, Qinghua Hu, Xiao Wang, and Qilong Wang. CCP-GNN: Compet-
729 itive covariance pooling for improving graph neural networks. *IEEE Transactions on Neural Net-*
730 *works and Learning Systems*, 2024. URL [https://doi.org/10.1109/TNNLS.2024.](https://doi.org/10.1109/TNNLS.2024.3390249)
731 [3390249](https://doi.org/10.1109/TNNLS.2024.3390249).
732
733
734
735
736
737
738
739
740
741
742
743
744
745
746
747
748
749
750
751
752
753
754
755

756	APPENDIX CONTENTS	
757		
758	A Future work	16
759		
760	B Related work	16
761		
762	C Notations and abbreviations	17
763		
764	D Additional preliminaries	17
765		
766	D.1 Pullback metrics	17
767		
768	D.2 Riemannian operators on the SPD manifold	18
769		
770	E Technical details on Riemannian Logarithm	18
771		
772	F Power-deformed GBWM as local power-AIM	20
773		
774	G Additional discussions on Pow-TMLR, Pow-EMLR, and ScalePow-EMLR	21
775		
776	G.1 The equivalence of Pow-EMLR and ScalePow-EMLR	21
777		
778	G.2 The in-equivalence of Pow-EMLR and Pow-TMLR	21
779		
780	G.3 A Riemannian perspective of Pow-TMLR vs. Pow-EMLR	21
781		
782	H Additional experimental details	22
783		
784	H.1 Datasets	22
785		
786	H.2 Implementation details	22
787		
788	I Proof of Thm. 2	23
789		
790	J Additional discussions on Thm. 2	25
791		
792		
793		
794		
795		
796		
797		
798		
799		
800		
801		
802		
803		
804		
805		
806		
807		
808		
809		

810 A FUTURE WORK

811
812 While Chen et al. (2024c) also explored Riemannian MLRs induced by other metrics, these MLRs
813 involve computationally expensive Riemannian computations, rendering them unsuitable for large-
814 scale datasets. As a future avenue, we aim to simplify the Riemannian computations in these alter-
815 native Riemannian classifiers and apply them to GCP for improved covariance matrix classification.
816

817 B RELATED WORK

818
819 **Global covariance pooling.** GCP aims to leverage the second-order statistics of deep features to
820 enhance the learning competence of DNNs. DeepO²P (Ionescu et al., 2015), acknowledged as the
821 first end-to-end global covariance pooling network, employs matrix logarithm for the classification
822 of covariance matrices. This method also offers matrix backpropagation to differentiate the gradient
823 w.r.t the decomposition-based matrix functions. Following this pioneering work, B-CNN (Lin et al.,
824 2015) employs the outer product of global features and carries out element-wise power normaliza-
825 tion. However, there exist three limitations of the above two methods. Firstly, the high dimensional
826 covariance feature considerably escalates the parameters of the FC layer, thereby introducing the
827 risk of overfitting. Secondly, the matrix logarithm could over-stretch the small eigenvalues, under-
828 mining the effectiveness of GCP. Thirdly, the matrix logarithm is based on matrix decomposition,
829 which is computationally expensive. The subsequent research primarily focuses on four aspects: (a)
830 adopting richer statistical representation (Wang et al., 2017; Zheng et al., 2019; Nguyen, 2021); (b)
831 reducing the dimensionality of the covariance feature (Gao et al., 2016; Kong & Fowlkes, 2017; Cui
832 et al., 2017; Acharya et al., 2018; Rahman et al., 2020; Wang et al., 2022a); (c) investigating effec-
833 tive and efficient matrix normalization (Li et al., 2018; Zheng et al., 2019; Lin & Maji, 2017; Yu
834 et al., 2020; Song et al., 2022c;b); (d) improving covariance conditioning for better generalization
835 ability (Song et al., 2022d;a). In this work, we do not aim to achieve state-of-the-art performance
836 over the existing GCP-based methods but rather to unravel the underlying theoretical mechanism of
837 GCP matrix functions.

838 **Interpretations of global covariance pooling.** Along with the progress of GCP, several works
839 began to study its mechanism. Wang et al. (2020b) investigated the effect of GCP on deep Convo-
840 lutional Neural Networks (CNNs) from an optimization perspective, including accelerated conver-
841 gence, stronger robustness, and good generalization ability. Wang et al. (2023) further broadened
842 these investigations, substantiating the merits of GCP in other networks, such as vision transform-
843 ers (Touvron et al., 2021; Yuan et al., 2021; Liu et al., 2021) and differentiable Neural Architecture
844 Search (NAS) (Liu et al., 2019). Song et al. (2021) empirically studied the advantage of approximate
845 matrix square root over the accurate one. Wang et al. (2022a) considered the matrix power as decor-
846 relating representations and developed a channel-adaptive dropout to produce lower-dimensional
847 covariance matrices. Nevertheless, existing literature does not fully address the fundamental ques-
848 tion of why Euclidean classifiers operate effectively in the non-Euclidean space generated by the
849 matrix power. Our research fills in this theoretical gap, offering intrinsic explanations regarding the
850 role of the matrix functions in GCP.

851 **Riemannian classifiers on SPD manifolds.** Since the matrix logarithm is a diffeomorphism be-
852 tween the SPD manifold and its tangent space at the identity (Arsigny et al., 2005), the most widely
853 used classifier on SPD manifolds is composed of the matrix logarithm and a Euclidean classifier
854 (Wang et al., 2021; Chen et al., 2023; Wang et al., 2022b; Nguyen, 2022a;b; Wang et al., 2022c;
855 Chen et al., 2024b; Wang et al., 2024). However, this tangent classifier might distort the intrinsic
856 geometry of SPD manifolds. Inspired by HNNs (Ganea et al., 2018), recent studies have devel-
857 oped intrinsic classifiers directly on SPD manifolds. Nguyen & Yang (2023) introduced three gyro
858 structures on SPD manifolds induced by AIM, LEM, and LCM, respectively. Based on these gyro
859 structures, the authors generalize the Euclidean Multinomial Logistics Regression (MLR). Concur-
860 rently, Chen et al. (2024a) proposed a formula for SPD MLR under Riemannian metrics pulled back
861 from the Euclidean space. However, both works require specific Riemannian properties and focus on
862 certain metrics on SPD manifolds. Chen et al. (2024c) presented a general framework for designing
863 Riemannian MLRs on general geometries and showcased their framework under various metrics on
864 SPD manifolds, covering the SPD MLRs introduced in (Chen et al., 2024a; Nguyen & Yang, 2023).
865 In this paper, based on the Riemannian classifiers developed in (Chen et al., 2024c), we present an
866 intrinsic explanation for matrix functions in GCP.

Table 7: Summary of notations.

Notation	Explanation
\mathcal{S}_{++}^n	The SPD manifold
\mathcal{S}^n	The Euclidean space of symmetric matrices
\mathcal{L}^n	The Euclidean space of $n \times n$ lower triangular matrices
$T_P \mathcal{S}_{++}^n$	The tangent space at $P \in \mathcal{S}_{++}^n$
$g_P(\cdot, \cdot)$ or $\langle \cdot, \cdot \rangle_P$	The Riemannian metric at $P \in \mathcal{S}_{++}^n$
$\langle \cdot, \cdot \rangle$ or $\cdot \cdot \cdot$	The standard Frobenius inner product
Log_P	The Riemannian logarithm at P
$H_{a,p}$	The Euclidean hyperplane
$f_{*,P}$	The differential map of f at $P \in \mathcal{S}_{++}^n$
f^*g	The pullback metric by f from g
$\text{ad}(\cdot)$	The adjoint operator of linear maps
ST	ST = $\{(\alpha, \beta) \in \mathbb{R}^2 \mid \min(\alpha, \alpha + n\beta) > 0\}$
$\langle \cdot, \cdot \rangle^{(\alpha, \beta)}$	The $O(n)$ -invariant Euclidean inner product
$g^{(\alpha, \beta)\text{-LE}}$	The Riemannian metric of (α, β) -LEM
$g^{(\alpha, \beta)\text{-AI}}$	The Riemannian metric of (α, β) -AIM
$g^{(\theta, \alpha, \beta)\text{-AI}}$	The Riemannian metric of (θ, α, β) -AIM
$g^{(\alpha, \beta)\text{-E}}$	The Riemannian metric of (α, β) -EM
$g^{(\theta, \alpha, \beta)\text{-E}}$	The Riemannian metric of (θ, α, β) -EM
$g^{(\theta_1, \theta_2)\text{-E}}$	The Riemannian metric of (θ_1, θ_2) -EM
g^{BW}	The Riemannian metric of BWM
$g^{M\text{-BW}}$	The Riemannian metric of M -BWM
$g^{(2\theta, M)\text{-BW}}$	The Riemannian metric of $(2\theta, M)$ -BWM
g^{LC}	The Riemannian metric of LCM
$g^{\theta\text{-LC}}$	The Riemannian metric of θ -LCM
f_{FC} or $\mathcal{F}(\cdot; A, b)$	The FC layer
Pow_θ or $(\cdot)^\theta$	The matrix power
f_{vec}	The vectorization
f_{EC}	A Euclidean classifier
mlog	The matrix logarithm
$\mathcal{L}_P[\cdot]$	The Lyapunov operator
Chol	The Cholesky decomposition
$\mathcal{L}_{P,M}[\cdot]$	The generalized Lyapunov operator
$\text{Dlog}(\cdot)$	The diagonal element-wise logarithm
f_M	The matrix function of matrix power or logarithm
$[\cdot]$	The strictly lower triangular part of a square matrix
$\mathbb{D}(\cdot)$	A diagonal matrix with diagonal elements from a square matrix

C NOTATIONS AND ABBREVIATIONS

For better clarity, we summarize all the notations in Tab. 7 and all the abbreviations in Tab. 8.

D ADDITIONAL PRELIMINARIES

D.1 PULLBACK METRICS

The power-deformed metrics on the SPD manifold are special cases of pullback metrics. Pullback metrics are common techniques in Riemannian geometry, connecting different Riemannian metrics.

Definition 3 (Pullback Metrics). Suppose \mathcal{M}, \mathcal{N} are smooth manifolds, g is a Riemannian metric on \mathcal{N} , and $f : \mathcal{M} \rightarrow \mathcal{N}$ is smooth. Then the pullback of g by f is defined point-wisely,

$$(f^*g)_p(V_1, V_2) = g_{f(p)}(f_{*,p}(V_1), f_{*,p}(V_2)), \quad (19)$$

where $p \in \mathcal{M}$, $f_{*,p}(\cdot)$ is the differential map of f at p , and $V_i \in T_p\mathcal{M}$. If f^*g is positive definite, it is a Riemannian metric on \mathcal{M} , which is called the pullback metric defined by f .

Table 8: Summary of Abbreviations.

Abbreviation	Explanation
SPD	Symmetric Positive Definite
GCP	Global covariance pooling
GAP	Global Average Pooling
LEM	Log-Euclidean Metric
AIM	Affine-Invariant Metric
EM	Euclidean Metric
PEM	Power Euclidean Metric
MPEM	Mixed Power Euclidean Metric
BWM	Bures-Wasserstein Metric
GBWM	Generalized Bures-Wasserstein Metric
FGVC	Fine-Grained Visual Categorization
MLR	Multinomial Logistics Regression
EMLR	Euclidean Multinomial Logistics Regression
RMLR	Riemannian Multinomial Logistics Regression
SPD MLR	RMLR on SPD manifolds
Log-EMLR	Eq. (4)
Pow-EMLR	Eq. (5)
Pow-TMLR	EMLR in the tangent space generated by Eq. (7)
ScalePow-EMLR	ScalePow-EMLR in Tab. 4
Cho-TMLR	EMLR in the tangent space generated by Eq. (8)

D.2 RIEMANNIAN OPERATORS ON THE SPD MANIFOLD

The $O(n)$ -invariant Euclidean inner product on \mathcal{S}^n (Thanwerdas & Pennec, 2023) is defined as

$$\langle V, W \rangle^{(\alpha, \beta)} = \alpha \langle V, W \rangle + \beta \operatorname{tr}(V) \operatorname{tr}(W), \quad (20)$$

where $(\alpha, \beta) \in \mathbf{ST}$ with $\mathbf{ST} = \{(\alpha, \beta) \in \mathbb{R}^2 \mid \min(\alpha, \alpha + n\beta) > 0\}$, $V, W \in \mathcal{S}^n$, and $\langle \cdot, \cdot \rangle$ is the standard matrix inner product.

We summarize deformed SPD metrics and associated Riemannian operators in Tab. 9 with the following notations. Specifically, $P, Q, M \in \mathcal{S}_{++}^n$ are SPD matrices, and V, W are tangent vectors in the tangent space at P , i.e., $T_P \mathcal{S}_{++}^n$. We denote $g_P(\cdot, \cdot)$ as the Riemannian metric at P , and $\operatorname{Log}_P(\cdot)$ as the Riemannian logarithm at P , respectively. Also, Chol and mlog represent the Cholesky decomposition and matrix logarithm, with their differential maps at P denoted as $\operatorname{Chol}_{*,P}$ and $\operatorname{mlog}_{*,P}$, respectively. We denote $\tilde{V} = \operatorname{Chol}_{*,P}(V)$, $\tilde{W} = \operatorname{Chol}_{*,P}(W)$, $L = \operatorname{Chol}(P)$, and $K = \operatorname{Chol}(Q)$. $[\cdot]$ is the strictly lower part of a square matrix, $\mathbb{D}(\cdot)$ is a diagonal matrix with diagonal elements of a square matrix, and $\operatorname{Dlog}(\cdot)$ is a diagonal matrix consisting of the logarithm of the diagonal entries of a square matrix. We denote $\mathcal{L}_{P,M}[V]$ as the generalized Lyapunov operator, i.e., the solution to the matrix linear system $M\mathcal{L}_{P,M}[V]P + P\mathcal{L}_{P,M}[V]M = V$. When $M=I$, $\mathcal{L}_{P,I}[V]$ is reduced to the Lyapunov operator, denoted as $\mathcal{L}_P[V]$.

E TECHNICAL DETAILS ON RIEMANNIAN LOGARITHM

We first review a well-known result for the pullback metric (Thanwerdas & Pennec, 2022, Tab. 2).

Lemma 4. *Given a Riemannian metric g on the SPD manifold \mathcal{S}_{++}^n and a diffeomorphism $f : \mathcal{S}_{++}^n \rightarrow \mathcal{S}_{++}^n$, the Riemannian logarithm $\tilde{\operatorname{Log}}_P$ under the pullback metric $\tilde{g} = f^*g$ is*

$$\tilde{\operatorname{Log}}_P Q = (f_{*,P})^{-1} \left(\operatorname{Log}_{f(P)} f(Q) \right), \quad (21)$$

where $f_{*,P}$ is the differential map at P , and Log is the Riemannian logarithm under g .

Next, we show a lemma about the scaling of a Riemannian metric.

Lemma 5. *Supposing \mathcal{S}_{++}^n is endowed with a Riemannian metric g and $a > 0$ is a positive real scalar, the scaling metric ag shares the same Riemannian logarithm map with g .*

Table 9: Riemannian operators and deformed metrics of seven basic metrics on SPD manifolds. Note that for MPEM, P and Q must be commuting matrices when computing the Riemannian logarithm.

Name	Riemannian Metric $g_F(V, W)$	Riemannian Logarithm $\text{Log}_P Q$	Deformation ($\theta \neq 0$)
(α, β) -LEM (Thanwerdas & Pennec, 2023)	$\langle \text{mlog}_{*,P}(V), \text{mlog}_{*,P}(W) \rangle^{(\alpha, \beta)}$	$(\text{mlog}_{*,P})^{-1} [\text{mlog}(Q) - \text{mlog}(P)]$	$\frac{1}{\theta^2} \text{Pow}_{\theta}^* g^{(\alpha, \beta)\text{-LE}}$
(α, β) -AIM (Thanwerdas & Pennec, 2023)	$\langle P^{-1}V, WP^{-1} \rangle^{(\alpha, \beta)}$	$P^{1/2} \text{mlog}(P^{-1/2}QP^{-1/2}) P^{1/2}$	$\frac{1}{\theta^2} \text{Pow}_{\theta}^* g^{(\alpha, \beta)\text{-AI}}$
(α, β) -EM (Thanwerdas & Pennec, 2023)	$\langle V, W \rangle^{(\alpha, \beta)}$	$Q - P$	$\frac{1}{\theta^2} \text{Pow}_{\theta}^* g^{(\alpha, \beta)\text{-E}}$
(θ_1, θ_2) -EM (Thanwerdas & Pennec, 2022)	$\frac{1}{\theta_1 \theta_2} \langle \text{Pow}_{\theta_1, *, P}(V), \text{Pow}_{\theta_2, *, P}(W) \rangle$	$(\text{Pow}_{\theta, *, P})^{-1}(Q^{\theta} - P^{\theta})$, with $\theta = (\theta_1 + \theta_2)/2$	N/A
LCM (Lin, 2019)	$\sum_{i>j} \tilde{V}_{ij} \tilde{W}_{ij} + \sum_{j=1}^n \tilde{V}_{jj} \tilde{W}_{jj} L_{jj}^{-2}$	$(\text{Chol}^{-1})_{*,L} [\lfloor K \rfloor - \lfloor L \rfloor + \mathbb{D}(L) \text{Dlog}(\mathbb{D}(L)^{-1} \mathbb{D}(K))]$	$\frac{1}{\theta^2} \text{Pow}_{\theta}^* g^{\text{LC}}$
BWM (Bhatia et al., 2019)	$\frac{1}{2} \langle \mathcal{L}_P[V], W \rangle$	$(PQ)^{1/2} + (QP)^{1/2} - 2P$	$\frac{1}{4\theta^2} \text{Pow}_{2\theta}^* g^{\text{BW}}$
GBWM (Han et al., 2023)	$\frac{1}{2} \langle \mathcal{L}_{P,M}[V], W \rangle$	$M(M^{-1}PM^{-1}Q)^{1/2} + (QM^{-1}PM^{-1})^{1/2}M - 2P$	$\frac{1}{4\theta^2} \text{Pow}_{2\theta}^* g^{M\text{-BW}}$

Proof. Since the Christoffel symbols of ag are identical to those of g , the geodesic functions under both ag and g remain unchanged. This implies that the Riemannian exponential maps are the same for ag and g . As the inverse of the Riemannian exponential maps, the Riemannian logarithm maps under ag and g are also identical. \square

By the above lemmas, we can readily prove Tab. 2.

Proof. By Lem. 5, for the power-deformed metric of a metric g in \mathcal{S}_{++}^n , the Riemannian logarithm at I is the same as the counterpart under $\text{Pow}_{\theta}^* g$. Therefore, in the following, without loss of generality, we compute Log_I under $\text{Pow}_{\theta}^* g$. We further denote the Riemannian logarithm under g as $\bar{\text{Log}}$.

In the following, we denote P as an SPD matrix, 0 as the $n \times n$ zero matrix, and V as a tangent vector in $T_I \mathcal{S}_{++}^n$. Besides, we note that

$$\text{Pow}_{\theta, *, I}(V) = \theta V. \quad (22)$$

We first deal with (α, β) -LEM and θ -LCM, as both of them are pullback metrics from the Euclidean space. Then, we proceed to deal with other metrics

(α, β) -LEM: As shown in (Thanwerdas & Pennec, 2023), the Riemannian logarithm at I is

$$\begin{aligned} \text{Log}_I(P) &= \text{mlog}_{*,I}^{-1}(\text{mlog}(P) - \text{mlog}(I)) \\ &= \text{mlog}(P). \end{aligned} \quad (23)$$

θ -LCM: We define a map as

$$f = \psi \circ \text{Chol} \circ \text{Pow}_{\theta}, \quad (24)$$

where $\psi(L) = \lfloor L \rfloor + \text{Dlog}(\mathbb{D}(L))$ for the lower triangular matrix L . Chen et al. (2024d) shows that LCM is the pullback metric by $\psi \circ \text{Chol}$ from the Euclidean space \mathcal{L}^n of lower triangular matrices. Therefore, $\text{Pow}_{\theta}^* g^{\text{LC}}$ is the pullback metric from \mathcal{L}^n by f . Besides, we have the following:

$$f(P) = \lfloor \tilde{L} \rfloor + \text{Dlog}(\mathbb{D}(\tilde{L})), \quad (25)$$

$$f(I) = 0, \quad (26)$$

$$f_{*,I}(V) = \theta \left(\lfloor V \rfloor + \frac{1}{2} \mathbb{D}(L) \right), \quad (27)$$

where $\tilde{L} = \text{Chol}(P^{\theta})$. We have

$$\begin{aligned} \text{Log}_I(P) &= (f_{*,P})^{-1}(f(P) - f(I)) \\ &= \frac{1}{\theta} \left[\lfloor \tilde{L} \rfloor + \lfloor \tilde{L} \rfloor^{\top} + 2 \text{Dlog}(\mathbb{D}(\tilde{L})) \right]. \end{aligned} \quad (28)$$

For (θ, α, β) -EM, (θ_1, θ_2) -EM, (θ, α, β) -AIM, 2θ -BWM, and $(2\theta, P^{2\theta})$ -BWM, we denote Log_I as their logarithm at I , while $\bar{\text{Log}}_I$ as the logarithm under the metric before deformation. The results can be directly obtained by Eq. (22), Lem. 4, Lem. 5, and Tab. 9.

1026 (θ, α, β) -EM:

$$\begin{aligned}
 1027 \quad \text{Log}_I(P) &= \frac{1}{\theta} \bar{\text{Log}}_I(P^\theta) \\
 1028 & \\
 1029 &= \frac{1}{\theta} (P^\theta - I). \\
 1030 &
 \end{aligned} \tag{29}$$

1031 (θ_1, θ_2) -EM: The Log_I can be directly obtained by Tab. 9 and Eq. (22).

1032 (θ, α, β) -AIM:

$$\begin{aligned}
 1033 \quad \text{Log}_I(P) &= \frac{1}{\theta} \bar{\text{Log}}_I(P^\theta) \\
 1034 & \\
 1035 &= \frac{1}{\theta} \text{mlog}(P^\theta) \\
 1036 & \\
 1037 &= \text{mlog}(P). \\
 1038 &
 \end{aligned} \tag{30}$$

1039 2θ -BWM:

$$\begin{aligned}
 1040 \quad \text{Log}_I(P) &= \frac{1}{2\theta} \bar{\text{Log}}_I(P^{2\theta}) \\
 1041 & \\
 1042 &= \frac{1}{\theta} (P^\theta - I). \\
 1043 & \\
 1044 &
 \end{aligned} \tag{31}$$

1045 $(2\theta, P^{2\theta})$ -BWM: Under M -BWM, we have

$$1046 \quad \text{Log}_I(M) = 2(M^{\frac{1}{2}} - I). \tag{32}$$

1047 Therefore, for $(2\theta, P^{2\theta})$ -BWM, we have

$$\begin{aligned}
 1048 \quad \text{Log}_I(P) &= \frac{1}{2\theta} \bar{\text{Log}}_I(P^{2\theta}) \\
 1049 & \\
 1050 &= \frac{1}{\theta} (P^\theta - I). \\
 1051 & \\
 1052 & \\
 1053 &
 \end{aligned} \tag{33}$$

1054 □

1055 F POWER-DEFORMED GBWM AS LOCAL POWER-AIM

1056 Let us first formalize this property.

1057 **Proposition 6.** For any $P \in \mathcal{S}_{++}^n$ and $V, W \in T_P \mathcal{S}_{++}^n$, we have the following:

$$1061 \quad g_P^{(2\theta, P^{2\theta})\text{-BW}}(V, W) = \frac{1}{4} g_P^{(2\theta, 1, 0)\text{-AI}}(V, W). \tag{34}$$

1062 *Proof.* As shown in (Bhatia, 2009), the Riemannian metric of the standard AIM $((1, 1, 0)$ -AIM) is

$$1063 \quad g_P^{\text{AI}}(V, W) = \text{vec}(V)^\top (P \otimes P)^{-1} \text{vec}(W), \tag{35}$$

1064 where $\text{vec}(V)$ is the column vectorization of V , \otimes is the Kronecker product.

1065 For the $(2\theta, P^{2\theta})$ -BWM, we have the following:

$$\begin{aligned}
 1066 \quad g_P^{(2\theta, P^{2\theta})\text{-BW}}(V, W) &= \frac{1}{4\theta^2} g_{\tilde{P}}^{\phi_{2\theta}(P)\text{-BW}}(\tilde{V}, \tilde{W}) \\
 1067 & \\
 1068 &= \frac{1}{4} \cdot \frac{1}{4\theta^2} \text{vec}(\tilde{V})^\top (\tilde{P} \otimes \tilde{P})^{-1} \text{vec}(\tilde{W}) \\
 1069 & \\
 1070 &= \frac{1}{4} \cdot \frac{1}{4\theta^2} g_{\tilde{P}}^{\text{AI}}(\tilde{V}, \tilde{W}) \\
 1071 & \\
 1072 &= \frac{1}{4} g_P^{(2\theta, 1, 0)\text{-AI}}(V, W), \\
 1073 & \\
 1074 & \\
 1075 & \\
 1076 & \\
 1077 &
 \end{aligned} \tag{36}$$

1078 where $\tilde{V} = \text{Pow}_{2\theta^*, P}(V)$, $\tilde{W} = \text{Pow}_{2\theta^*, P}(W)$, $\tilde{P} = P^{2\theta}$, and Eq. (36) can be obtain by (Han
1079 et al., 2023, Eq. 3) □

G ADDITIONAL DISCUSSIONS ON POW-TMLR, POW-EMLR, AND SCALEPOW-EMLR

G.1 THE EQUIVALENCE OF POW-EMLR AND SCALEPOW-EMLR

It can be proven that Pow-EMLR is equivalent to ScalePow-EMLR under scaled initial weight and learning rate in the FC layer. We denote the network as

$$x_0 \in \mathbb{R}^{d_0} \xrightarrow{g(\cdot; \Theta)} x \in \mathbb{R}^d \xrightarrow{f_{\text{FC}}} y \in \mathbb{R}^c \rightarrow L \in \mathbb{R}, \quad (37)$$

where x_0 , $g(\cdot; \Theta)$, f_{FC} , and L are the input feature, feature extraction with parameter Θ , FC layer, and loss, respectively. The FC layers in Pow-EMLR and ScalePow-EMLR are denoted as $y = Ax + b$ and $\bar{y} = \frac{1}{\theta} \bar{A} \bar{x} + \bar{b}$. We set the initial values and learning rates of A and \bar{A} satisfying $A_0 = \frac{1}{\theta} \bar{A}_0$ and $\bar{\gamma} = \theta^2 \gamma$, and maintain all the other settings the same. Then, we have the following for the gradient at $A = A_0$ (or $\bar{A} = \bar{A}_0$):

$$\begin{aligned} \frac{\partial L}{\partial \bar{A}} &= \frac{1}{\theta} \frac{\partial L}{\partial \bar{y}} \bar{x}^\top = \frac{1}{\theta} \frac{\partial L}{\partial y} x^\top = \frac{1}{\theta} \frac{\partial L}{\partial A}, \\ \frac{\partial L}{\partial \bar{x}} &= \frac{1}{\theta} \bar{A}^\top \frac{\partial L}{\partial \bar{y}} = A^\top \frac{\partial L}{\partial y} = \frac{\partial L}{\partial x}. \end{aligned} \quad (38)$$

Under SGD, the updated values of \bar{A} satisfying the following:

$$\begin{aligned} \frac{1}{\theta} \bar{A}_1 &= \frac{1}{\theta} (\bar{A}_0 + \bar{\gamma} \frac{\partial L}{\partial \bar{A}}) \\ &= \frac{1}{\theta} (\bar{A}_0 + \bar{\gamma} \frac{1}{\theta} \frac{\partial L}{\partial A}) \\ &= \frac{1}{\theta} \bar{A}_0 + \bar{\gamma} \frac{1}{\theta^2} \frac{\partial L}{\partial A} \\ &= A_0 + \gamma \frac{\partial L}{\partial A} \\ &= A_1. \end{aligned} \quad (39)$$

Therefore, the updated values of A and \bar{A} still satisfy $A_1 = \frac{1}{\theta} \bar{A}_1$. In addition, the gradients of Pow-EMLR w.r.t. x and b are identical to ScalePow-EMLR w.r.t. \bar{x} and \bar{b} . Therefore, Pow-EMLR is equivalent to ScalePow-EMLR under scaled settings.

G.2 THE IN-EQUIVALENCE OF POW-EMLR AND POW-TMLR

We denote $X = S^\theta$. Then for Pow-TMLR, we have the following

$$\begin{aligned} y &= \mathcal{F} \left(f_{\text{vec}} \left(\frac{1}{\theta} (X + I) \right); A, b \right) \\ &= \mathcal{F} \left(f_{\text{vec}} (X + I); \tilde{A}, \tilde{b} \right) \\ &= \mathcal{F} \left(f_{\text{vec}} (X); \tilde{A}, \tilde{b} \right), \end{aligned} \quad (40)$$

where $\tilde{A} = \frac{1}{\theta} A$ and $\tilde{b} = \frac{1}{\theta} A f_{\text{vec}}(I)$.

As A appears in \tilde{b} , the gradient of A is composed of two parts, one w.r.t. y and the other one w.r.t. \tilde{b} . In contrast, in the standard FC layer $y = \mathcal{F}(X; A, b)$, the gradient of A is independent of b . Therefore, Pow-TMLR cannot be simply viewed as equivalent to Pow-EMLR with transformed initialization.

G.3 A RIEMANNIAN PERSPECTIVE OF POW-TMLR VS. POW-EMLR

Although the numerical expressions of Pow-TMLR and Pow-EMLR differ by a constant transformation, they differ fundamentally in theory: Pow-TMLR is a tangent classifier, whereas Pow-EMLR is a Riemannian classifier.

1. **Tangent Classifier:** The tangent classifier treats the entire manifold as a single tangent space at the identity matrix. When mapping data into this tangent space, critical structural information, such as distances and angles, cannot be preserved. This distortion undermines classification performance. In contrast, Riemannian MLR is constructed based on Riemannian geometry, fully respecting the manifold’s geometric structure.
2. **Tangent as a Special Case of Riemannian Classifier.** The tangent classifier can be seen as a reduced case of the Riemannian classifier. For example, let us take Eq. (16) as an example. When all SPD parameters P_k are set to the fixed identity matrix, Eq. (16) exactly corresponds to Pow-TMLR.

In summary, the Riemannian classifier enjoys significant theoretical advantages over the tangent classifier while incorporating the tangent classifier as a special case.

H ADDITIONAL EXPERIMENTAL DETAILS

H.1 DATASETS

The Caltech University Birds (Birds) (Welinder et al., 2010) dataset is composed of 11, 788 images distributed over 200 different bird species. The FGVC Aircrafts (Aircrafts) (Maji et al., 2013) dataset comprises 10, 000 images of 100 classes of airplanes, while the Stanford Cars (Cars) (Krause et al., 2013) dataset consists of 16, 185 images representing 196 classes of cars. In addition to these widely used FGVC datasets, we also evaluate our proposed theory on the large-scale ImageNet-1k (Deng et al., 2009) dataset, which contains 1.28M training images, 50K validation images and 100K testing images distributed across 1K classes.

H.2 IMPLEMENTATION DETAILS

We follow the official Pytorch code of iSQRT-COV¹ (Li et al., 2018) to reimplement GCP. Following (Wang et al., 2020a; Song et al., 2022a), we use ResNet-18 as our backbone network on the ImageNet dataset, and ResNet-50 on the other three FGVC datasets. On Both the ImageNet-1k and FGVC datasets, the ResNet-18 and ResNet-50 are trained from scratch with the GCP layer.

Following (Song et al., 2022a), we reduce the channels of the final convolutional features from 2048 to 256 for compact representation of covariance matrices, producing 256×256 spatial covariance matrices. We train the network from scratch with an SGD optimizer on all datasets. For a fair comparison, the learning settings are identical for Pow-EMLR and ScalePow-EMLR. The learning rate is set as $1e^{-1.1}$, $5e^{-3}$, $5e^{-2}$, and $5e^{-2}$ for the convolutional layers on the ImageNet, Aircrafts, Birds, and Cars dataset. The learning rate of the FC layer is set to be 5, 10 and 10 times larger than the convolutional layers for the Aircrafts, Cars, and Birds datasets, respectively. We impose a weight decay of $1e^{-4}$ on the optimizer on four datasets. On the Aircrafts dataset, the training lasts 50 epochs with the learning rate divided by 5 at epoch 20. On the Cars and Birds datasets, the training lasts 100 epochs with a learning rate reduction by a divisor of 10 at epoch 50.

As the matrix square root is the most effective matrix function in GCP, we set power = $1/2$ for matrix power normalization.

The experiments on ImageNet use a workstation with 32-core AMD EPYC 7302 CPU and an NVIDIA RTX A6000, while other experiments use a workstation with 16-core AMD EPYC 7302 CPU and an NVIDIA GeForce RTX 2080 Ti GPU. Due to the heavy computational burden of Cholesky decomposition, we do not implement Cho-TMLR on the ImageNet.

For Cho-TMLR, the learning rate is set as $1e^{-2}$, $5e^{-3}$, and $3e^{-3}$ for the convolutional layers on the Aircrafts, Birds, and Cars dataset. The batch size on the Cars dataset is 4. On the Aircrafts dataset, the training lasts 60 epochs with the learning rate divided by 5 at epoch 50. On the Cars and Birds datasets, the training lasts 120 epochs with a learning rate reduction by a divisor of 10 at epoch 100. Other settings remain the same as the ones in the main paper.

¹<https://github.com/jiangtaoxie/fast-MPN-COV>

For Pow-TMLR, the learning rate is set as $1e^{-1.1}$ and $5e^{-3}$ for the convolutional layers on the ImageNet and the other three FGVC datasets. The batch size on the Cars dataset is set as 6. Other settings remain the same as the ones in the main paper.

H.3 EXPERIMENTS ON THE SECOND-ORDER TRANSFORMER

Table 10: Comparison of Pow-EMLR, ScalePow-EMLR and Pow-TMLR under the SoT-7 backbone on the ImageNet-1k dataset.

Classifier	Top-1 Acc (%)	Top-5 Acc (%)
Pow-TMLR	75.79	92.91
ScalePow-EMLR	76.14	93.18
Pow-EMLR	76.11	93.05

To further validate our findings, we follow Song et al. (2022b) to conduct experiments using the Second-order Transformer (SoT) (Xie et al., 2021) on the ImageNet-1k dataset. Specifically, we use the 7-layer SoT (SoT-7) architecture as the backbone network and train the model up to 250 epochs with a batch size of 512, keeping the other settings the same as Song et al. (2022b).

As shown in Tab. 10, Pow-EMLR still achieves similar performance to ScalePow-EMLR, but outperforms Pow-TMLR. These results further support our claim that tangent classifiers cannot adequately explain the matrix functions used in GCP, while the underlying mechanism can be better explained by our Riemannian perspective.

I PROOF OF THM. 2

This proposition is mainly inspired by Thm. 5 in (Chen et al., 2024a). However, all the results in (Chen et al., 2024a) require the metric to be a pullback metric from a *standard Euclidean space*, while the metric in our Thm. 2 is a pullback metric from *the SPD manifold*. Nevertheless, we still can reach similar theoretical results. We first recap RSGD and then begin to present our proof.

RSGD (Bonnabel, 2013) is formulated as

$$\bar{W} = \text{Exp}_W(-\gamma \Pi_W(\nabla_W f)) \quad (41)$$

where Exp_W is the Riemannian exponential map at W , and Π_W maps the Euclidean gradient $\nabla_W f$ to the Riemannian gradient, and γ denotes learning rate.

We denote (1, 0)-EM as EM, and the metric tensor of it as g^E . Instead of providing an ad hoc proof exclusively for PEM, we present the following two more general lemmas.

Lemma 7. *Given a diffeomorphism $\phi : \mathcal{S}_{++}^n \rightarrow \mathcal{S}_{++}^n$, ϕ induces a pullback metrics on \mathcal{S}_{++}^n from $\{\mathcal{S}_{++}^n, g^E\}$, denoted as $g^{\phi-E}$. The $g^{\phi-E}$ -induced SPD MLR is*

$$p(y = k|S) \propto \exp[\langle \phi(S) - \phi(P_k), \phi_{*,I}(A_k) \rangle], \quad (42)$$

where $S \in \mathcal{S}_{++}^n$ is an input feature, $P_k \in \mathcal{S}_{++}^n$ and $A_k \in \mathcal{S}^n$ are parameters for each class k .

Proof. According to Chen et al. (2024c, Thm. 3.3), the Riemannian MLR based on $g^{\phi-E}$ is given as

$$\begin{aligned} p(y = k|S) &\propto \exp \left[g_{P_k}^{\phi-E}(\text{Log}_{P_k} S, \text{PT}_{I \rightarrow P_k} A_k) \right] \\ &= \exp[\langle \phi(S) - \phi(P_k), \phi_{*,I}(A_k) \rangle], \end{aligned} \quad (43)$$

where Eq. (43) can be obtained by the properties of deformed metrics (Thanwerdas & Pennec, 2022, Tab. 2) and EM (Thanwerdas & Pennec, 2023, Tab. 3). \square

Following the notations in Lem. 7, we have the following lemma.

Lemma 8. *Supposing $\phi_{*,I}$ is the identity map and each SPD parameter P_k (Euclidean parameter A_k) in Eq. (42) is optimized by $g^{\phi-E}$ -based RSGD (Euclidean SGD), the $g^{\phi-E}$ -based SPD MLR is equivalent to a Euclidean MLR illustrated in Eq. (10) in the co-domain of ϕ .*

1242 *Proof.* We first show the projection operator Π_P at $P \in \mathcal{S}_{++}^n$ under $g^{\phi-E}$, and then move on to the
 1243 equivalence.

1244 For any smooth function $f : \mathcal{S}_{++}^n \rightarrow \mathbb{R}$ on \mathcal{S}_{++}^n endowed with $g^{\phi-E}$, we denote its Euclidean and
 1245 Riemannian gradient at $P \in \mathcal{S}_{++}^n$ as $\nabla_P f$ and $\tilde{\nabla}_P f$, respectively. Then, for any $V \in T_P \mathcal{S}_{++}^n$, we
 1246 have

$$\begin{aligned} 1247 \langle \tilde{\nabla}_P f, V \rangle_P = V(f) &\Rightarrow \langle \phi_{*,P} \tilde{\nabla}_P f, \phi_{*,P} V \rangle = \langle \nabla_P f, V \rangle \\ 1248 &\Rightarrow \Pi_P(\nabla_P f) = \phi_{*,P}^{-1} \circ (\text{ad}(\phi_{*,P}))^{-1} (\nabla_P f), \end{aligned} \quad (44)$$

1250 where $\text{ad}(\cdot)$ is the adjoint operator of the linear map.

1251 According to Eq. (10), we define a Euclidean MLR in the codomain of ϕ as

$$1253 p(y = k | S) \propto \exp(\langle \phi(S) - \bar{P}_k, \bar{A}_k \rangle), \text{ with } \bar{P}_k, \bar{A}_k \in \mathcal{S}^n. \quad (45)$$

1254 We call this classifier ϕ -EMLR.

1255 Following Lem. 7, the SPD MLR under $g^{\phi-E}$ is

$$1257 p(y = k | S) \propto \exp(\langle \phi(S) - \phi(P_k), \tilde{A}_k \rangle), \text{ with } P_k \in \mathcal{S}_{++}^n, \tilde{A}_k \in \mathcal{S}^n. \quad (46)$$

1259 Supposing the SPD MLR and ϕ -EMLR satisfying $\bar{P}_k = \phi(P_k)$. Other settings of the network are
 1260 all the same, indicating the Euclidean gradients satisfying

$$1262 \frac{\partial L}{\partial \bar{P}_k} = \frac{\partial L}{\partial \phi(P_k)}. \quad (47)$$

1264 The updates of \bar{P}_k in the ϕ -EMLR is

$$1266 \bar{P}'_k = \bar{P}_k - \gamma \frac{\partial L}{\partial \bar{P}_k}. \quad (48)$$

1268 The updates of P_k in the SPD MLR is

$$\begin{aligned} 1269 P'_k &= \text{Exp}_{P_k}(-\gamma \Pi_{P_k}(\nabla_{P_k} f)) \\ 1270 &= \phi^{-1} \left[\phi(P_k) - \gamma (\text{ad}(\phi_{*,P}))^{-1} \left(\frac{\partial L}{\partial P_k} \right) \right]. \end{aligned} \quad (49)$$

1274 Therefore $\phi(P'_k)$ satisfies

$$\begin{aligned} 1275 \phi(P'_k) &= \phi(P_k) - \gamma (\text{ad}(\phi_{*,P}))^{-1} \left(\frac{\partial L}{\partial P_k} \right) \\ 1276 &= \phi(P_k) - \gamma (\text{ad}(\phi_{*,P}))^{-1} \circ \text{ad}(\phi_{*,P_k}) \left(\frac{\partial L}{\partial \phi(P_k)} \right) \\ 1277 &= \phi(P_k) - \gamma \frac{\partial L}{\partial \phi(P_k)} \\ 1278 &= \bar{P}'_k. \end{aligned} \quad (50)$$

1284 The second equation comes from the Euclidean chain rule of differential. Let $Y = \phi(X)$, then we
 1285 have

$$\begin{aligned} 1286 \frac{\partial L}{\partial Y} : dY &= \frac{\partial L}{\partial Y} : \phi_{*,X}(dX) \\ 1287 &= \text{ad}(\phi_{*,X}) \left(\frac{\partial L}{\partial Y} \right) : dX, \end{aligned} \quad (51)$$

1290 where $\cdot : \cdot$ means Frobenius inner product.

1291 The equivalence of \bar{A}_k and \tilde{A}_k is obvious. Since both forward and backward processes of Eq. (45)
 1292 and Eq. (46) are identical, by natural induction, the lemma can be proven. \square

1294 When $\theta > 0$, simple computation shows that $(\theta, 1, 0)$ -EM is the pullback metric of EM by ϕ_θ with
 1295 $\phi_{\theta*,I}$ as an identity map. According to Lems. 7 and 8, one can readily prove Thm. 2.

J ADDITIONAL DISCUSSIONS ON THM. 2

In Lem. 8, $\phi_{*,I}$ is required to be identity map. However, Lem. 8 can be extended into the case where $\phi_{*,I}$ is not the identity map, which will further extend Thm. 2 into the case of $\theta < 0$.

Following the notations in Lem. 7, let $\phi : \mathcal{S}_{++}^n \rightarrow \mathcal{S}_{++}^n$ be a diffeomorphism, whose differential at I , i.e., $\phi_{*,I}$ is not an identity map. As ϕ is a diffeomorphism, the differential map $\phi_{*,I} : T_I \mathcal{S}_{++}^n \rightarrow T_{\phi(I)} \mathcal{S}_{++}^n$ is a linear isomorphism, i.e., a bijection preserving linear operations. Therefore, we can identify $\tilde{A}_k = \phi_{*,I}(A_k)$ with A_k in Eq. (42), and the SPD MLR under $g^{\phi-E}$ is simplified as

$$p(y = k|S) \propto \exp \left[\langle \phi(S) - \phi(P_k), \tilde{A}_k \rangle \right], \quad (52)$$

where $\tilde{A}_k \in \mathcal{S}^n$. As a direct corollary, all the proof in Lem. 8 can be transferred to the case where $\phi_{*,I}$ is not an identity.

Corollary 9. *Supposing $\phi : \mathcal{S}_{++}^n \rightarrow \mathcal{S}_{++}^n$ is a diffeomorphism and each SPD parameter P_k (Euclidean parameter A_k) in Eq. (52) is optimized by $g^{\phi-E}$ -based RSGD (Euclidean SGD), the $g^{\phi-E}$ -based SPD MLR is equivalent to a Euclidean MLR in the co-domain of ϕ .*

As a direct application of Cor. 9, Thm. 2 can be generalized into the case of $\theta < 0$. We generalize the definition of ϕ_θ as

$$\phi_\theta(S) = \frac{1}{|\theta|} S^\theta, \forall S \in \mathcal{S}_{++}^n, \text{ with } \theta \neq 0. \quad (53)$$

Obviously, $\phi_\theta : \mathcal{S}_{++}^n \rightarrow \mathcal{S}_{++}^n$ is still a diffeomorphism. By Cor. 9, we can readily obtain the following results.

Corollary 10. *Under PEM with $\theta \neq 0$, optimizing each SPD parameter P_k in Eq. (52) by PEM-based RSGD and Euclidean parameter A_k by Euclidean SGD, the PEM-based SPD MLR is equivalent to a Euclidean MLR illustrated in Eq. (10) in the co-domain of $\phi_\theta(\cdot)$.*

Rahman et al. (2023) adopted the inverse of the covariance matrix for GCP. Cor. 10 indicates that our framework can also explain the underlying mechanism of the inverse in (Rahman et al., 2023).